UCRL-ID-129568

Enhancing Environmental Restoration Predictive Modeling in Undersampled Environments

Robert J. Gelinas
John P. Ziagos
Said K. Doss
Robert G. Nelson*

*PDE Solutions, Inc.

Submitted as Final LDRD Report

March 25, 1998

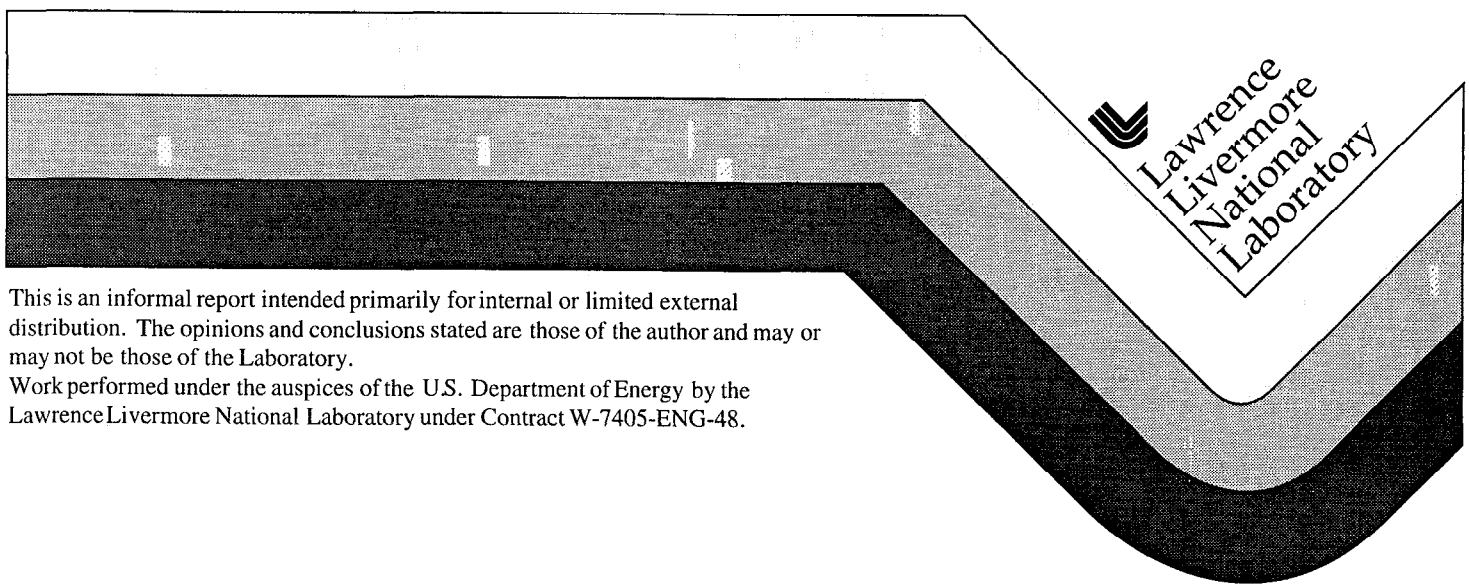

Work performed under the auspices of the U.S. Department of Energy by the Lawrence Livermore National Laboratory under Contract W-7405-ENG-48.

DISCLAIMER

Work performed under the auspices of the U.S. Department of Energy by Lawrence Livermore National Laboratory under Contract W-7405-Eng-18.

Enhancing Environmental Restoration Predictive Modeling in Undersampled Environments

ABSTRACT

New computational physics methods for estimating constitutive property parameterizations in ground water aquifers were developed and demonstrated in this project. The dynamical and statistical axioms of physics, embodied in partial differential equations (PDEs) of kinetic theory, are employed to constrain interpolations of hydraulic head (pressure) and transmissivity (permeability) between sparsely measured datum points. These methods can apparently be applied in numerous approaches to parameter estimation. To demonstrate the basic concepts and techniques developed in this work, examples are considered for steady-state, two-dimensional, heterogeneous, ground water flow models, given (i) discrete borehole observations of hydraulic head and transmissivity and (ii) governing kinetic equations for Darcy flow behavior. Estimations of spatially dependent parameters from sparsely measured data are treated as mathematically ill-posed problems because infinitely many parameter distributions (realizations) that are consistent with the data generally exist. Potential difficulties associated with ill-posedness in mean flow realizations are mitigated by requiring that acceptable realizations respect the observed data, are solutions of forward and inverse PDEs for physical continuity, respect information sampling principles, and are distributed by spatial interpolations that themselves are optimal solutions of the governing PDEs between measured datum points.

To accomplish these requisites, adaptive numerical grid Galerkin techniques were applied in a novel manner—one that calibrates (constrains) the forward and inverse PDE solutions to assume the observed values of head and transmissivity at measurement locations, while also interpolating the PDE solutions between the measurement locations with basis functions, optimizations, and adaptive grids that are indigenous to Galerkin methods. Long-standing problems associated with data sampling and noise were mitigated by introducing and solving additional regularizing PDEs that, in effect, spatially filter data interpolations simultaneously with the solution of data-constrained forward and inverse flow PDEs, commensurate with information sampling and signal processing principles.

Applications of these estimation techniques to synthetic data sets with known analytic solutions demonstrate attainable accuracy levels of the techniques in challenging problems and, more importantly, provide examples of the genuine effects of data undersampling, which is always an important factor in actual practice. Finally, practical realizations of aquifer transmissivity are computed for a field data set obtained in Superfund cleanup activities at Lawrence Livermore National Laboratory's Livermore Site.

1.0 INTRODUCTION

The design and fielding of ground water remediation systems is an imposing and expensive technical problem that is being addressed in the United States and many other countries around the world. Computer model simulations of subsurface contaminant flow and transport are used extensively to assist in the development of these designs. They are used further to forecast and analyze the total time and cost for remediation under alternative engineering options, risk levels, and/or various stakeholder-driven options. Results of appropriate data-calibrated simulations can

be pivotal in decision-making because they provide perhaps the most rational basis for estimating future aquifer behavior, potential health risks, possible compliance alternatives, and potential outcomes of contingency actions throughout the life of a remediation project. On the other hand, results of simulations may be only as good (or poor) as the constitutive property parameterizations used in the flow simulation model.

Reliability of aquifer simulations depends directly on the amount and quality of information for hydraulic and subsurface rock properties (e.g., permeability and porosity). The great expense of drilling and sampling fluid and rock properties nearly always result in severe undersampling of the subsurface. So there is a considerable premium for extracting the greatest amount of information contained in any given amount of data, as well as for gathering the right types of data at optimal locations in the first instance. These are all tasks in the arena of parameter estimation, which critically depends on solutions of inverse problems. The power of advanced adaptive modeling methods employed here, to both spatially filter and interpolate measured data with rigorously constrained forward and inverse kinetic PDE solutions, has barely been tapped in existing parameter estimation techniques. Yet no other modeling advances—in computer speed and memory, massively parallel performance, enhanced visualization technology, statistical methods, etc., can overcome the shortcomings caused by constitutive parameters that fail to simulate observed data according to underlying requisites of physics and mathematics, consistent with signal processing principles (Bracewell, 1986; McGillem and Cooper, 1984).

Viewed broadly, inverse problems are found in all of science and engineering where hypotheses are repeatedly tested and revised with theory and calculations in order to explain observations or guide the collection of data in the future. This is always an iterative, or indirect, calibration process, necessitated by fundamental uncertainties inherent in physical measurements and conceptual parameterizations. Because spatially variable material properties, or constitutive parameters, can never be perfectly sampled and measured, their distribution is always non-unique and is thus estimated by a repetitive circular process, until consistency is achieved with measurements of related dependent variables. This is good news and bad news. The bad news is such problems are inherently ill-posed, because an indefinite number of parameter realizations that are consistent with sparsely measured data generally exist. The good news is this ill-posedness does not imply that the parameter estimation process is meaningless. It indicates that well-founded concepts of mathematics and physics must be applied and executed successfully, in order to generate multiple well-posed realizations that are suitably calibrated to available data. Parameter estimation methods differ widely in the techniques that are used to generate realizations between measured datum points. The multiple realizations are then processed further, either internally or a posteriori to determine the 'best solutions' for satisfying specific problem objectives. The fundamental circular process of parameter estimation is respected in the present work by simultaneously coupling the inverse modeling of constitutive parameters with the forward modeling of dependent variables through data calibrations. Many techniques that may be used to measure 'fitness' or to select those parameter realizations that represent 'best solutions' can be found in the technical literature (Menke, 1989; Parker, 1994; Datta-Gupta *et al.* 1997), and are not included in the scope of this project.

Owing to the fact that subsurface media are severely undersampled by borehole measurements on macroscopic and regional scales, hydrologists have contended for several decades with the difficulties of non-uniqueness and ill-posedness in inverse solutions of aquifer parameters. Parameter estimation theories of various types have been advanced and applied over that time in not

only ground water management but also contaminant remediation, oil and gas recovery, and mining industries. Extensive reviews and seminal articles on parameter estimation methods in heterogeneous porous media can be found and examined in the technical literature. A small sampling would include publications by Stallman (1958); Nelson (1961, 1962); Frind and Pinder (1973); Gelhar (1993); Dagan (1989); Yeh (1986); Neuman (1973, 1980, 1982); Clifton and Neuman (1982); Carrerra and Neuman (1986a, 1986b); Sun (1994); and McLaughlin and Townley (1996).

The purpose of this project is to develop and apply new computational physics techniques for estimating single-phase saturated flow parameters from measured data in ground water aquifers in order to help improve forecasts of ground water flow and contaminant movement. A related goal is to reduce unnecessarily large uncertainties by eliminating nonphysical artifacts in existing estimation methods. The new techniques developed in this project became possible by exercising cumulative advances that have materialized over many years in dynamic unstructured adaptive numerical grid methods for solving nonlinear systems of partial differential equations (PDEs). These adaptive methods have now been integrated with automated code generators so that technical practitioners can rapidly formulate and construct complete codes with advanced self-controlled numerical solution methods for diverse problems (Backstrom, 1994, 1998; Gelinas *et al.* 1995; Nelson, 1998). More than one hundred entirely new codes (not simply incremental versions of a previous code) were constructed and executed in this project. With this mode of modeling, many alternative physics approaches, PDE systems, mathematical formulations, field data formulations, and spatial filtering techniques were posed and tested over a three-year period. All of the hands-on coding work in that time interval was performed by one scientific practitioner, at approximately 70% of full-time effort.

The parameter estimation techniques in this report were developed as an application of fundamental kinetic theory, where aquifer parameters are directly represented stochastically through their average properties. That is, a hierarchical system of deterministic kinetic equations describes the evolution of mean values, average fluctuation intensities, and average cross-correlations. (Averaged stochastic variables beyond second-order are usually truncated in ground water applications.) The full hierarchical system of kinetic equations can sometimes be solved simultaneously and calibrated with measured data. Or, in other instances, the hierarchy of kinetic flow equations is decoupled into low- and higher-order equation systems, which are then solved and calibrated with measurements using a combination of numerical PDE methods (for the low-order forward and inverse equations) and functional analysis techniques (for the higher-order statistical averages). Because every direct and indirect parameter estimation method depends, first of all, on the quality of parameters estimated in the mean flow equation, the kinetic hierarchy in the present work was truncated beyond first-order in order to keep matters as simple as possible and describe essential advances that apply, first, at the lowest-order of kinetic hierarchies. It is expected that these techniques will also find beneficial application in existing random field (Langevin) and manual history-matching methods. Major differences between the techniques reported here and those applied previously in the mean flow portion of stochastic parameter estimation methods reside in several factors, which include advanced sparse data calibrations/interpolations, additional mathematical and physical continuity constraints, spatial filtering, and noise-minimization procedures. By resolving long-standing critical problems in this project, techniques for obtaining and utilizing higher-order statistical properties from kinetic theory can be examined more cogently in future efforts. This report is organized as follows: 1.0 Introduction; 2.0 Background and

Problem Definition; 3.0 Description of Methods; 4.0 Application and Results; 5.0 Concluding Remarks.

2.0 BACKGROUND AND PROBLEM DEFINITION

To emphasize basic concepts without a significant loss of generality, steady-state ground water flow in a confined aquifer is modeled according to Darcy's law over regional scales. The steady ground water flow equation in three spatial dimensions (3-D) can be written as:

$$\nabla \bullet (K\nabla h) + Q = 0, \tag{2.1}$$

where K is the hydraulic conductivity of the aquifer, ∇h is the hydraulic head gradient, and Q represents internal source and sink rates. When the aquifer thickness is substantially smaller than the horizontal scale of the flow domain, the two-dimensional (2-D) flow equation

$$\nabla \bullet (T\nabla h) + Q = 0, \tag{2.2}$$

is a reasonable approximation for many aquifers. The transmissivity T is defined as the product of K and the aquifer thickness, b. (Unless otherwise noted, we exercise an understood convention in subsurface flow articles of using scalar notation for tensor quantities, e.g., K and T in this report.) A site characterized by borehole measurements of hydraulic head and transmissivity is depicted schematically in Figure 1. There are measurements of hydraulic head and transmissivity at discrete locations in the domain, Ω, and on its boundaries $\partial\Omega$. The thickness of the aquifer is assumed to be known from measurements, as are pumping sources and sink rates in equations (2.1) and (2.2). Transmissivity data are usually more sparse than head data. Head measurements are usually much more accurate and localized at the borehole than are transmissivity values. For convenience in this initial work, Q is henceforth taken to be zero.

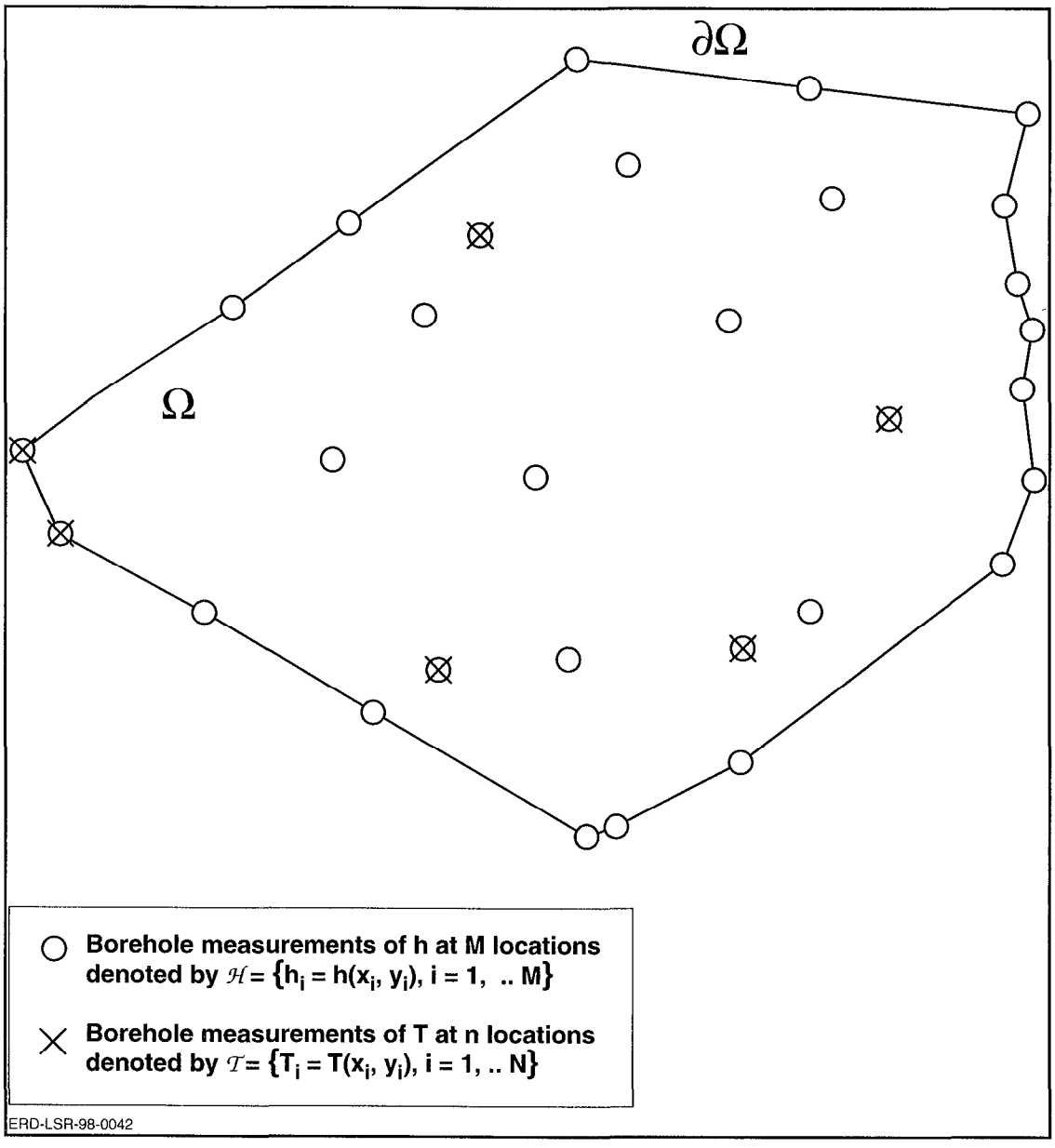

Figure 1: Remediation site domain Ω with boundary ∂Ω, characterized by discrete borehole meausrements of h and T.

The principal problem that faces remediation analysts is, *How to construct h(x,y) and T(x,y) solutions everywhere in a domain from sparse, discrete, noisy measurements in order to best calibrate, forecast, and otherwise interpret flow behavior according to the PDE of Equation (2.2)?*

A specific physics formulation of the forward and inverse problem is a first pre-requisite in parameter estimation. Several formulations are possible. For example, one may ask, is h(x,y) in equations (2.1) and (2.2) a random statistical variable, a mean (ensemble) flow variable, or a tacitly undefined variable? Also, is the flow equation (2.2) to be taken as a stochastic (Langevin) equation, a mean flow equation, or an unspecified deterministic equation? All of these optional

formulations have been investigated to various extents over the past forty years of aquifer parameter estimation research. Although a comprehensive review of previous work is not feasible here, it is useful to sketch some of the major eras and trends of inverse problem developments for aquifer parameter estimation, in more or less chronological order.

Early efforts (in the 1950s–1970s) to estimate hydraulic properties of an aquifer focused largely upon the mathematical problem of solving the inverse flow equations (2.1) and (2.2) (Stallman, 1958; Nelson, 1961, 1962; Frind and Pinder, 1973; Emsellem and deMarsily, 1971; Haddamard, 1952; and many others); also see discussions in texts by Dagan (1989) and Gelhar (1993). The flow equation was tacitly considered to be a PDE for mean variables in a physical continuum, usually without explicit mention of its kinetic physics context. For the forward (elliptic PDE) problem T, Q, and boundary conditions are known, and h is unknown. It is a direct, well-posed problem. The inverse (first-order hyperbolic PDE) problem seeks to solve the same mean flow equation but with h and Q given and with T the unknown. This is usually a much more difficult problem to solve because of its tendency to become ill-posed. That is, when h(x,y) is known in a domain, one value of T on each streamline defines all other values of T on that streamline. Transmissivity values on different streamlines are mathematically independent because T on one streamline is not related to T on any other streamline. Transmissivities on different streamlines are however interrelated by a boundary condition on so-called Cauchy curves (Γs), which intersect every streamline in a 2-D domain. Solution of the inverse flow PDE on streamlines with Cauchy datum points is a direct, well-posed problem. But, Nelson (1961) noted that, when an average value of T is used in some sub-region to represent what is really a transmissivity distribution on a continuum of streamlines, inconsistencies can be expected because a single permeability value cannot be completely descriptive of a nonuniform distribution. General solutions for T(x,y) on an (infinite) continuum of streamlines were not practically attainable, given transmissivity data on Cauchy curves and noisy head data over the entire problem domain during that era. The difficulties associated with such mathematical inconsistencies/instabilities when attempting to fill physical space with either continuum or zonally averaged transmissivities, exacerbated by noisy undersampled head data and fixed numerical grid methods for solving flow PDEs, were well recognized but pursued nonetheless for many years with limited success. From a physics standpoint, the inverse problem was addressed primarily as a dynamics problem because model and data calibrations seeking to respect both dynamical and statistical axioms in a coherent kinetic physics context were generally lacking in this early era of ground water modeling investigations.

Recognition that more effective statistical techniques were needed led next to applications of least-squares optimization techniques from control theory. Objective function minimizations that respected sparsely measured data according to methods from control theory were implemented in user-ready codes (Doherty, 1990, among others). These techniques, referred to as indirect methods, were driven primarily by multiple forward model solutions. The forward flow equation was most often tacitly considered to be a PDE for mean variables in a physical continuum. With few exceptions (e.g., Zhu, 1992) the inverse flow PDE was not solved, or otherwise respected mathematically, in conjunction with the forward solutions used in objective function minimizations. Incrementations of forward model simulations sufficed to generate Jacobians that are used in the functional minimizations, without respecting the Cauchy conditions of the inverse PDE. Practical difficulties were encountered in numerical robustness, stability, and economy. But

the principal shortcoming was that, by failing to satisfy Cauchy criteria of the inverse PDE, transmissivity parameter realizations failed to respect physical continuity.

It became widely recognized by the 1980s that it is expedient to represent aquifer parameters stochastically through their average properties, which include mean values, average intensity of fluctuations, and correlations. (Kitinades and Vomvoris, 1983; Newman and Yakowitz, 1979; Newman, 1980; Clifton and Neuman, 1982, and many others.) Two major stochastic approaches are available and have been used extensively in diverse technical disciplines for several decades. One approach is probabilistic characterization, which determines the joint probability distribution function (pdf) of any set of spatially dependent random variables (e.g., head, permeability, and other hydrogeologic parameters). Master equations (Carle and Fogg, 1996; Carle, 1996), as well as Liouville equations of classical and quantum physics, describe the dynamic evolution of pdf's. These types of pdf methods are not considered in the present work. The other major stochastic approach is kinetic theory. It may either develop and solve systems of deterministic PDEs in a physical continuum for statistical properties (which include mean values, average intensity of fluctuations, and average cross-correlations) or determine the statistical properties by employing functional techniques for random fields in conjunction with the mean PDE. The random field functional techniques have apparently predominated over the kinetic PDE techniques in subsurface flow parameter estimation problems to date. A recent article by McLaughlin and Townley (1996) presents a well-balanced analysis that shows how some of the various functional concepts and methods, which frequently use 'most probable' or maximum a posteriori estimates, are interrelated.

The functional approaches that are applied in subsurface parameter estimations can be classified broadly as Langevin methods. (See for example, articles by Lax, 1966; Akcasu and Osborn, 1966). The basic premise in ground water systems is that the flow equation (2.2) is a stochastic equation, with stochastic variables defined by:

$$h(x,y) = \langle h(x,y) \rangle + h'(x,y) \tag{2.3}$$

$$T(x,y) = \langle T(x,y) \rangle + T'(x,y) \tag{2.4}$$

$$q(x,y) = \langle q(x,y) \rangle + q'(x,y). \tag{2.5}$$

The variables denoted with angular brackets are mean moments, and the primed variables account for fluctuations from various possible sources, including measurement errors, unaccounted physical processes (e.g., diurnal stresses) and undersampling errors in a physical system. Ensemble averages of the primed random variables in equations (2.3)–(2.5) are zero. Numerical PDE solution errors have sometimes been included as fluctuation sources in parameter estimation methods. They are not considered in the present work because dynamic adaptive grid methods are designed to yield user-specified accuracy levels that can be quite high, relative to the fixed-grid solution methods that have been used so widely in ground water models to date.

When equations (2.3)–(2.5) are substituted into the stochastic equation (2.2) and the resulting equation is averaged, a type of Langevin equation is obtained. Its terms can be assembled into two groupings of variables: one grouping is composed of only mean variables; and the second

grouping is composed of only terms that contain averages of products of primed variables. The first grouping is the conventional mean flow PDE; and the remaining fluctuation terms are sometimes referred to as 'equivalent noise sources.' It is here where Langevin and kinetic PDE approaches usually part ways and use somewhat different mathematical representations and solution techniques to estimate ground water parameters. Both approaches must replace an ill-posed problem by schemas that solve well-posed problems. Kinetic PDE methods solve a well-posed hierarchy of PDEs for multiple realizations that respect measured data for averaged moments of h, T, and various products (e.g., h^2, T^2, hT, etc.). Langevin methods employ either phenomenological analyses or well-posed 'estimator' operators with functional analysis techniques to determine statistical properties of h, T, and Q for 'most probable' property distributions that are consistent with experimental observations. The estimators replace a theoretical inverse operator, which generally doesn't exist due to non-uniqueness, for the mapping of hydraulic head measurements to estimates of transmissivities (McLaughlin and Townley, 1996). Although constrained by the forward mean flow equation, randomly distributed transmissivity realizations are unconstrained by solutions of the inverse mean flow equation in practice. As a result, most geostatistical (including kriging, co-kriging, etc.) and Langevin methods of parameter estimation fill space with randomly distributed transmissivities that are evidently not conditioned to respect physical continuity requisites at the lowest order of the kinetic hierarchy of averaged moments. (The work of Neuman and Orr (1993) in non-Darcy flow models, and possibly some other investigators, can apparently accommodate the conditioning of randomly prescribed transmissivity distributions with the inverse mean PDE constraint applied compatibly with the forward mean PDE.) Some of the techniques developed in the present work may thus find additional application in random field approaches that can accommodate conditioning of parameter realizations with *both* forward and inverse mean flow PDEs.

Kinetic equations can be derived from both axiomatic physics foundations (Ono, 1954, 1959; Osborn, 1963; Osborn and Natelson, 1965; Gelinas, 1966, 1967) and phenomenologically with Langevin techniques (Akcasu, 1966; Osborn, 1967; Gelinas, 1976). Diverse technical applications of these two basic kinetic approaches have ranged over atomic to astrophysical scales in space and time. The kinetic theory represented by average moment equation hierarchies makes no assumptions about the statistical distributions of h and T. The evolution equations for averaged moments (of various h and T products) are derived directly from the underlying dynamical equation for the probability distribution function without having to know or estimate the pdf itself. The statistical properties of h and T are then the dependent variables in a hierarchy of deterministic kinetic equations. Whereas the lowest-order (mean) equations are solved more or less routinely in practical applications, simultaneous solutions of the extended hierarchical system of first- and second-order average moment equations are generally more difficult to solve. If the full hierarchical system is not solved simultaneously, the higher-order average moments may nonetheless be used to constrain and select, a posteriori, the 'best solutions' generated from data-calibrated kinetic PDEs.

The mean kinetic PDE that corresponds to equation (2.2) for flow in porous media with no sources or sinks can be written as:

$$\nabla \bullet (\langle T \rangle \nabla \langle h \rangle + \langle T' \nabla h' \rangle) = 0 \qquad (2.6)$$

A kinetic PDE in which the cross-correlation term, $\langle T' \nabla h' \rangle$, is the dependent variable can be written functionally as:

$$L_1(\langle T' \nabla h' \rangle) = f_1(\langle T \rangle, \langle h \rangle, \langle T' T' \rangle, \langle h' h' \rangle). \quad (2.7)$$

Similarly the PDEs for variances that complete the hierarchy at second-order are written as:

$$L_2(\langle T' T' \rangle) = f_2(\langle T \rangle, \langle h \rangle, \langle T' h' \rangle, \langle h' h' \rangle), \quad (2.8)$$

$$L_3(\langle h' h' \rangle) = f_3(\langle T \rangle, \langle h \rangle, \langle T' h' \rangle, \langle T' T' \rangle), \quad (2.9)$$

where the operators L_1, L_2, and L_3 represent the left-hand sides of the higher-order moment equations (2.7 – 2.9); and the right-hand sides of these PDEs are represented by the functions f_1, f_2, and f_3.

When transmissivity depends significantly upon hydraulic head, as in partially saturated media, simultaneous solution and calibration of the coupled equations (2.6)–(2.9) to field data is generally required for best results. When the cross-correlation term in equations (2.6) is Fickian, the kinetic hierarchy is separable in the sense that the mean flow equation (2.6) reduces to the following expression, which resembles the original form of equation (2.2),

$$\nabla \bullet (\langle T \rangle \nabla \langle h \rangle) = 0. \quad (2.10)$$

In this instance, the higher-order moments may depend on mean variables, but the mean variables do not depend on the higher-order moments. The mean and higher-order moments can then be calibrated to measured data by separate techniques without loss of generality. For example, the forward and inverse mean PDE solutions can be calibrated to h and T data in multiple realizations over plausible ranges of uncertainty, on the one hand; and higher statistical moments from mean realizations can be calibrated to the measured data as an additional constraint for selecting realizations that best meet problem objectives, on the other hand.

In other cases, where the cross-correlation term in equation (2.6) is either sufficiently small (e.g., steady Darcy flow conditions in saturated media where transmissivity is assumed to be a function of only rock properties, independent of hydraulic head) or is known independently from other analyses (e.g., other functional approaches), the hierarchy may again be solved in a separable manner. The developments in the remainder of this report apply to equation (2.10) to illustrate essential principles, which can then be extended to more general cases in future efforts.

3.0 DESCRIPTION OF METHODS

The main task in this section is to present some practical methodologies that are capable of constructing transmissivity distributions everywhere in a domain Ω, based on knowledge of measured hydraulic head and transmissivity at a discrete and finite subset of Ω (see Figure 1). Such reference data is assumed to fairly conform with the model assumptions of a steady-state condition of an aquifer region with no internal ground water sources or sinks. The case with non-zero sources/sinks is being investigated in separate work; and it is a substantially more difficult

problem to solve numerically, especially when the given Q-term contains a collection of 'point sources/sinks.' Because the present work focuses on the mathematical model for the lowest-order (mean) equations of the kinetic hierarchy, the angle brackets for statistical averages in Section 2.0 will henceforth be dropped for convenience. Also, to facilitate subsequent discussions, the following definitions are introduced here, referring to Figure 1.

$\mathcal{S}$ A finite set of 2-D cartesian coordinates $\{(x_i,y_i), i = 1, 2, ...\}$ at which measurements of hydraulic head are collected. This 'fixed point set' becomes part of the nodal assembly in the finite element solution of the governing PDEs.

$\mathcal{H}$ The set of measured head values on the set $\mathcal{S}$.

$\mathcal{H}'$ Is constructed from $\mathcal{H}$ by replacing all elements of $\mathcal{H}$ by those obtained from the somewhat smoothed solution h_s in equation (3.7).

$\mathcal{T}$ A set of transmissivities inferred from other well tests at some subset of $\mathcal{S}$. These will be referred to as transmissivity measurements.

Ω A domain in the x-y plane over which one attempts to solve for h and T and whose boundary $\partial\Omega$ is a polygon consisting of those linear segments joining the 'outermost' points of the set $\mathcal{S}$.

$\mathcal{S}'$ All points of $\mathcal{S}$ which are not included in $\partial\Omega$; $\mathcal{S}' = \mathcal{S} - \partial\Omega$.

Ω' The entire domain excluding the set $\mathcal{S}$; $\Omega' = \Omega - \mathcal{S}$.

$C^n(\Omega)$ The class of all continuously differentiable functions in Ω up to order n.

Notice that it is always possible to construct Ω so that it is the convex hull of $\mathcal{S}$. However, such smallest convex set containing the set $\mathcal{S}$ could be inadequate in two main respects: First, highly acute boundary corners are generated when some of the outermost points of $\mathcal{S}$ are very remote in relation to the bulk of the remaining points; this is usually fixed by simply eliminating those remote points from $\mathcal{S}$ that would seriously degrade the solution in more important regions of the domain. Second, the number of boundary segments may be too small to allow for a reasonably accurate prescription of boundary conditions for h. More refinement of the boundary can frequently be attained by slightly relaxing the convexity condition on Ω and incorporating nearby points of $\mathcal{S}$ in the prescription of $\partial\Omega$. The proximity of nearby points of $\mathcal{S}$ to $\partial\Omega$ is usually measured relative to the diameter of $\mathcal{S}$.

Starting from the mean flow equation (2.10) for porous media with Q = 0,

$$\nabla \bullet (T\nabla h) = 0, \tag{3.1}$$

and assuming that h(x,y) is known everywhere in Ω, then equation (3.1) can in principle be solved for T(x,y) as the unknown dependent variable. This is the inverse solution process and is to be contrasted with the familiar usage of equation (3.1) to solve a forward problem for h when T is given everywhere in Ω. Frequently, equation (3.1) is referred to as the inverse equation when the inverse solution process is being considered; its solution, T, is then referred to as the inverse solution. Being a first order PDE in T, equation (3.1) can be solved by the method of characteristics provided that its coefficients satisfy some reasonable smoothness conditions.

Although the classic characteristic approach is not employed in this work; the latent wealth of information pertaining to the theory of first order partial differential equations (Courant and Hilbert, 1953; John, 1982) is nonetheless employed extensively and implicitly in the present work.

Sparsely measured head data (as well as sparse transmissivity data) present both the major problem and the reason for transmissivity parameter estimation. Because of the lack of complete knowledge of h everywhere in Ω, it follows, that head gradients are not defined in all of Ω; and thus a PDE simply does not exist from which T can be determined. An immediate way to proceed, then, is to find an interpolating surface that passes through all of the head datum points. Because a vast number of such surfaces often exist, one finds that, unless further constraints are imposed, the inverse solution (if found) will often yield unphysical transmissivity distributions. The cause of this difficulty is readily explained: most trial interpolating surfaces that pass through the measured head datum points form relative maxima or minima 'spikes' on the set S, thereby violating the maximum-principle for elliptic differential equations. See, for example, Protter and Weinberger (1984). The interpolating surfaces must therefore be selected judiciously—which is the starting point for the developments in this work.

Before forging ahead with the issue of how to construct and solve the inverse PDE, it is constructive to review briefly the method of characteristics for first-order quasi-linear differential equations. In order to write equation (3.1) in standard form, one assumes, momentarily, that the head, h, belongs to the class of functions $C^2(\Omega)$. The theory of characteristics then leads one to solve the following set of autonomous ordinary differential equations (ODEs):

$$\frac{dx}{ds} = \frac{\partial h}{\partial x} \tag{3.2}$$

$$\frac{dy}{ds} = \frac{\partial h}{\partial y} \tag{3.3}$$

$$\frac{dT}{ds} = -T\Delta h \tag{3.4}$$

where s is a parameter measured from some given 'initial' point (x_0,y_0,T_0), and Δ denotes the laplacian operator. The first two ODEs (3.2) and (3.3) easily map the geometry of characteristic curves (or more precisely, the projection of the characteristic curves on the x-y plane) based solely on knowledge of head gradients. The third ODE determines T uniquely along the entire characteristic which passes through (x_0,y_0) and such that $T=T_0$ at $s=0$. In fact, if the parametric solutions: $x=x(s,x_0,y_0)$, $y=y(s,x_0,y_0)$ obtained from equations (3.2) and (3.3) are substituted into equation (3.4), the solution to equation (3.4) is obtained readily in the form

$$T = T_0 \exp\{-\int_0^s \{\Delta h(\tau)\, d\tau\}, \tag{3.5}$$

which incidentally guarantees that T will always remain positive, as expected. It is assumed in equation (3.5) that the functional form of Δh is known at least along the characteristic curve through (x_0,y_0). Transmissivities would be completely determined everywhere in Ω once T is given values along an entire non-characteristic initial curve Γ, provided that all of the characteristic

curves emanating from Γ sweep the entire domain Ω. If not, one can only solve for T on the subdomain that is swept out by the characteristic curves.

Turning attention to the reality of dealing with non-smooth h, several daunting problems and concerns must be addressed at this stage. The first problem, the satisfactory resolution of head laplacians from sparse data, is in practice intractable because the head gradients are often discontinuous on Ω; and the head laplacian is therefore undefined on all of Ω. A second concern is that only one transmissivity value is needed on a characteristic curve in order to determine all other transmissivity values along that curve uniquely. If additional inconsistent values were to be assigned somehow on the same characteristic curve, as is frequently done in stochastic transmissivity parametrizations, zonation schemes, and history matching techniques, fundamental ODE solution requirements for the inverse equation are contradicted and physical continuity is not respected.

A third problem is one of managing logistics; i.e., the bookkeeping of all generated characteristic curves emanating from some finite set of points traversing Γ for the eventuality of constructing the integral surface containing these characteristic curves. Thoughts concerning these problems motivated the present quest for more viable parameter estimation techniques—techniques that can solve simultaneous forward and inverse flow PDEs, augmented by spatial filtering PDEs for data smoothing, in a true physical continuum according to kinetic theory.

The process developed here for heading off some of the classic difficulties mentioned above is composed of four basic steps. Each step can be described and verified separately before merging them finally into a simultaneous, iterative process for sparse, noisy data in field applications. The basic steps are:

1. Form a trial interpolating surface $h_r(x,y)$ in Ω such that, on the discrete subset $\mathcal{S}'$ of Ω, h_i is forced to take on the corresponding measured values in the set $\mathcal{H}$. The interpolator employed here is a variant of the flow equation.
2. Introduce and solve an additional PDE for smoothing h_i in Ω. The amount of smoothing of spikes in h_i at measurement points is controlled by user-selected parameters. This produces spatially filtered distributions h_s that can deviate from $\mathcal{H}$ on the set $\mathcal{S}'$ by any preset amount.
3. Introduce and solve two additional PDEs that produce smoothed head gradient components, u and v, from h_s obtained above. It is extremely important to smooth head gradients prior to using them as coefficients in the inverse equation.
4. Solve a regularized variant of the inverse equation using a spatially filtered head gradient (u,v) in lieu of ∇h.

The first step is a 'rough' interpolation of the hydraulic head data. The key idea is to bring a stronger influence of physical dynamics to bear on the interpolation, than is usually applied in statistical interpolation methods. An obvious choice is to use a variant of the mean flow PDE, itself, as the interpolator. Letting T be a constant average value (or any constant value), the interpolating equation is

$$\nabla\bullet(T\nabla h_i) = 0. \tag{3.6}$$

It is important to note that equation (3.6) is to be satisfied in Ω', rather than in the entire domain Ω. The solution h_i is 'pinned,' or clamped, to the set $\mathcal{H}$ on the remaining set $\mathcal{S}'$. In other words, h_i is constrained to both respect the values of measured head and to satisfy the flow equation everywhere else in Ω. This is directly analogous to solving mechanical stress problems with fixed loads at given coordinates. Galerkin numerical solution methods are especially well-suited for solving these types of PDEs because they can respect the data at fixed points and yield optimized solutions that minimize PDE residuals over the rest of the problem domain. On $\partial\Omega$, Dirichlet boundary conditions are assigned to h_i; these are calculated by linearly interpolating between the values of h at the known end-points of each boundary segment. Linear interpolation is expedient but other methods of assignment may be used when they are more appropriate.

This first trial interpolating surface is calculated in this work by employing a dynamic adaptive grid finite element code toolkit, PDEase, which enables the user to solve equation (3.6) in Ω', subject to the pinning constraints. (This feature was implemented in our version of the PDEase toolkit by its author, R.G. Nelson, specifically for this project. See the texts of Backstrom (1994, 1998) for not only specific information about using such advanced toolkits as PDEase but also new modes of thinking and posing computational models with these emerging tools that will increasingly respect and enforce essential mathematical requisites in complex physical problems.)

The solution h_r in this step is expected to possess relative maxima or minima that may be associated with several possible origins. First to come to mind is the sweeping approximation of replacing T by its average value on Ω. While this might seem to be the major cause for such extraneous behavior, it is seldom the case. Other possible causes include: data errors or noise, ground water sources/sinks that were previously unknown, absence of a perfect steady-state in nature, and local/non-Darcy effects (equivalent sources).

The second step performs an additional smoothing process on h_i over Ω in order to damp or completely diminish spurious spikes. It is necessitated because complete clamping of h_r to $\mathcal{H}$ on $\mathcal{S}'$ created a corresponding set of local spikes, which cannot exist anywhere in Ω, in the absence of physical sources or sinks. (When such spikes actually turn out to be previously unknown physical sources or sinks, the presently described techniques turn out to be useful 'source-finders,' which is another subject that will be considered as part of 'data-mining' in future work.) Looking ahead to the next (third) step, much of the important information content from hydraulic head measurements, no matter how sparse or devoid of high spatial frequency information they may be, resides in the gradients and laplacians of the head, as was indicated in previous discussion. The objective in the second and third steps is to extract as much information as possible by performing spatial filtering that is commensurate with the spatial frequencies of the measured data. Such filtering is also required to produce a smoothed h_s that effectively satisfies the maximum principle for elliptic differential equations. The clamping imposed on h_r is therefore relaxed at the measurement points by solving the following PDE for h_s on Ω:

$$\Delta h_s + \alpha (h_i - h_s) = 0 \quad \text{in} \quad \Omega. \tag{3.7}$$

The laplacian operation in the first term of equation (3.7) is recognized to be a bandpass filter function (McGillem and Cooper, 1984). It does not have a sharp cut-off at any spatial frequency; so some latitude can be exercised in laplacian smoothing with this factor in mind. The second term in equation (3.7) can be viewed as a penalty function that controls the amount of smoothing of h_r

through proper choices of the parameter α. Clearly, very large α yields an h_s that hardly differs from h_t; that is, very little smoothing is done. And vice versa, as α approaches zero, h_s approaches a harmonic solution in Ω. But too much smoothing is obviously undesirable when it loses (by aliasing) significant amounts of information about the set $\mathcal{H}$ on $\mathcal{S}$ '. So one must ask, how much/little smoothing should be applied at measured points? Simply stated, spikes in h_t at measurement points must be damped sufficiently so that only mild relative maxima and minima may still persist at this stage. (Recall that the average transmissivity assumed in the first step is not the final distribution that is sought.) The solution h_s is then used to construct a new set $\mathcal{H}$ ' of smoothed heads on $\mathcal{S}$', and $\mathcal{H}$' replaces $\mathcal{H}$ in subsequent steps.

The rationale for step three is built on the fact that the *gradient* of h_s, and not h_s per se, is the critical determinant in solving for T in step four. Because small deviations of h_s from a correspondingly true head produce large deviations in calculated head gradient, this smoothing step is mandatory. The principle applied in the third step is similar to that in step two. Defining (u,v) to be the desired smoothed head gradients, relative to less-smooth gradients $(\partial h_s/\partial x, \partial h_s/\partial y)$, the following two PDEs are introduced and solved for on Ω:

$$\Delta u + \beta\left(\frac{\partial h_s}{\partial x} - u\right) = 0 \quad \text{in} \quad \Omega, \tag{3.8}$$

$$\Delta v + \beta\left(\frac{\partial h_s}{\partial y} - v\right) = 0 \quad \text{in} \quad \Omega. \tag{3.9}$$

Several options are plausible for assigning boundary conditions (BCs) for u and v on $\partial\Omega$. A straightforward option is to let (u,v) take on the gradient of h_s on $\partial\Omega$. This option will generally produce solutions that behave unrealistically in the vicinity of $\partial\Omega$. This can easily be explained, since ∇h_s is generally discontinuous on $\partial\Omega$. If ∇h_s is first smoothed prior to employing it as given Dirichlet data, then a more realistic filtered solution (u,v) everywhere in Ω is expected. Another option that also tends to damp such peculiar behavior is a Neumann condition of the third type. This is the option used in present work.

The fourth step attempts to determine T based on knowledge of spatially filtered head gradient (u,v) obtained in step three. As part of a procedure that deals mainly with solutions of boundary value problems (BVPs) in steps 1-3, it is both desirable and advantageous to recast the inverse equation so that a BVP can be prescribed here as well. This is accomplished by solving a regularized version of equation (3.1) through the addition of the regularizing term $\varepsilon\Delta T$, for sufficiently small ε,

$$\nabla \bullet (Tu, Tv) + \varepsilon\Delta T = 0 \quad \text{in} \quad \Omega. \tag{3.10}$$

This modified equation (3.10) is in principle an elliptic equation. But in practice it is essentially a hyperbolic PDE. The solution to equation (3.10) can then be completely determined, provided that T is given along some non-characteristic curve Γ in the closure of Ω and such that the continuum of characteristics emanating from Γ span the entire domain Ω. For brevity, a Γ curve that satisfies these conditions will be referred to as an admissible Γ curve. If no admissible Γ curve exists for the entire domain Ω, then one must partition Ω into two or more subdomains, each of

which possesses its own admissible Γ curve. Fortunately, in the absence of sources and sinks in ground water flow problems the geometry of characteristic curves is usually simple enough (but not trivial!) that it only requires the specification of a single admissible Γ curve. No further specification of T along the remainder of $\partial\Omega$ is required. Such a 'no specification' boundary condition is exacted by recycling integrands in all boundary integrals that are produced from integration by parts in the numerical solution process. That is, whatever expression appears in a boundary integral, it is reused, as is, in forming the mass matrix of the Galerkin equations.

It appears, so far, that knowledge about the projection of the characteristic curves on the x-y plane (or simply characteristics) for equation (3.10) with $\varepsilon = 0$, enters in this analysis for the end purpose of determining admissible curves Γ. Such a purpose could just as well be accomplished quickly by graphically investigating the normalized spatially filtered head gradient (u/s, v/s), $s = (u^2 + v^2)^{0.5}$ (i.e., vector field plot). Knowledge about the characteristics, and more importantly how stably and efficiently they are determined, serve a much wider goal in this work. Consider, then, the solution ψ of the following first order PDE:

$$u\frac{\partial\psi}{\partial x} + v\frac{\partial\psi}{\partial y} = 0 \quad \text{in} \quad \Omega \tag{3.11}$$

and suppose Γ is an admissible curve in Ω, which could be a part of $\partial\Omega$. For simplicity, let ψ take on any monotonically increasing set of values along Γ, say for instance $\psi = s$, s being some parameterization of Γ such that $0 \le s \le 1$ (see Figure 2). One can conclude from the theory of characteristics that the continuum of curves $\{\psi = C,\ 0 \le C \le 1\}$ is precisely the set of all characteristic curves for equation (3.11). That is, if one can solve equation (3.11) 'directly' in Ω in lieu of actually solving the standard ODEs for the characteristic curves, namely,

$$\frac{dx}{ds} = u, \quad \frac{dy}{ds} = v, \tag{3.12}$$

the entire geometry of characteristics is then obtained, all at once, from the knowledge of ψ. Such direct solution of equation (3.11) can be accomplished by regularization with the term $\varepsilon\Delta\psi$, paralleling the previous discussion. The essential BC required here is that which is given along Γ, namely $\psi = s$; and 'no specification' BC is required along the remainder of $\partial\Omega$. The function ψ should not be confused with the classical stream function ϕ. The latter is defined as a solution to the Cauchy-Reimann equations,

$$\frac{\partial\phi}{\partial x} = \frac{\partial h}{\partial y} \cong v \tag{3.13a}$$

$$\frac{\partial\phi}{\partial y} = -\frac{\partial h}{\partial x} \cong -u \tag{3.13b}$$

and is usually obtained as the solution to the harmonic equation $\Delta\phi = 0$ along with proper choices of BC for ϕ on $\partial\Omega$. The solution ϕ obtained this way is identical to ψ only for constant T. Notice further that, since equations (3.13) also yield an equation similar to (3.11), namely,

$$u \frac{\partial \phi}{\partial x} + v \frac{\partial \phi}{\partial y} = 0, \tag{3.14}$$

it follows that ϕ obtained from equation (3.14) will be identical to ψ under similar specifications along Γ, regardless of the spatial distribution of T.

Returning to equation (3.10), it is of interest to note its relationship to equation (3.11). For simplicity assume that both u and v are differentiable. Equation (3.10) can then be written for $\varepsilon = 0$ as,

$$u \frac{\partial T}{\partial x} + v \frac{\partial T}{\partial y} + T \left(\frac{\partial u}{\partial x} + \frac{\partial v}{\partial y}\right) = 0. \tag{3.15}$$

In the absence of the last term (which is essentially $T\Delta h$), equation (3.15) is identical to equation (3.11) with ψ replaced by T. The point to be made here is that the behavior of the solution process in (3.11) is expected to reflect on how the solution process to (3.15) will develop. In fact, it was found that it is often convenient to represent T in (3.10) as the product of two functions,

$$T = \Phi T_g, \tag{3.16}$$

where T_g is a general or generic solution to equation (3.10) with $T_g = 1$ on Γ; and Φ is a particular solution to equation (3.11) with $\Phi = T_\gamma$ along Γ. It is clear from this specification that $T = T_\gamma$ on Γ. That the factorized form of T in equation (3.16) formally satisfies (3.10) is also straightforward to deduce. One can further notice that (u,v) only needs to be continuous along Γ in order for the representation (3.16) to make sense. Also notice that, if Γ is either a portion of the domain boundary $\partial\Omega$ or if it is an isocontour h(x,y) = constant, then no assumptions about the smoothness of (u,v) along Γ are required. The additional rationale for the T factorization will be addressed shortly.

The foregoing analysis of the four main steps was presented as sequential steps so that each succeeding step builds on the results of the preceding one, but not vice-versa. The core algorithm presented in this work, however, consists of merging, with slight modification, the equations studied in these steps into a full-fledged system of coupled nonlinear equations. The purpose of the sequential presentation was to: (i) better understand the motivations and rationale leading to the creation and execution of each step; (ii) derive a new set of head values $\mathcal{H}'$ that are more compatible with prospective transmissivity distributions than $\mathcal{H}$; and (iii) obtain a reasonably good starting set of trial values for the quartic {h, u, v, T}.

The system of equations employed for the final determination of T is derived with few minor modifications from the four steps discussed previously. The system solved in this final stage consists of four PDEs in four unknowns {h, u, v, T} expressed as:

$$\nabla \bullet T \nabla h = 0, \tag{3.17a}$$

$$\Delta u + \alpha\left(\frac{\partial h}{\partial x} - u\right) = 0, \tag{3.17b}$$

$$\Delta v + \alpha\left(\frac{\partial h}{\partial y} - v\right) = 0, \tag{3.17c}$$

$$\nabla \bullet (Tu, Tv) + \beta \Delta T = 0. \tag{3.17d}$$

The main distinction between equations (3.17) and the previous individual steps is that equation (3.6) with constant average T in step 1 is replaced by equation (3.17a), with *both* T and h unknown. A similar distinction holds between equation (3.17d) and equation (3.10). Whereas equation (3.17d) treats T, u, and v as unknowns, equation (3.10) was solved only for T with u and v assumed known. Notice that no further smoothing of h, itself, is performed here. The smoothing of head gradients is however, retained. Discussions related to boundary conditions in the previous steps carry over to this system of coupled equations, with one exception. Namely, the set $\mathcal{H}$ in step one is replaced by the set $\mathcal{H}'$ here. Taken as a whole, the system of PDEs (3.17) is obviously nonlinear in the unknown variables {h, u, v, T}. As such, it is important to start with good initial trial estimates according to the procedures developed in this work for starting the Newton-Raphson linearization process employed in the numerical PDE solver.

As discussed previously for equation (3.16), one can factorize T as $T = \Phi T_g$ and solve the system (3.17) with T_g in place of T, obtaining solutions for u, v, and T_g. One can then obtain Φ by solving separately, the following regularized PDE:

$$u\frac{\partial \Phi}{\partial x} + v\frac{\partial \Phi}{\partial y} + \varepsilon \Delta \Phi = 0. \tag{3.18}$$

The system (3.17) with T replaced by T_g is devoid of any particular assignment of transmissivity data along Γ. (Recall that $T_g = 1$ along Γ under this factorization.) The system (3.17) therefore needs to be solved only once; and many different possible realizations of T along Γ can then be tested quickly by solving the simpler, single equation (3.18). The facility of $T_g = 1$ on Γ implies that a reasonable initial guess for the Newton-Raphson linearization could be taken as $T_g = 1$ everywhere in Ω. On the other hand, an assignment of highly varying T along Γ when solving the original unfactorized T can lead to instabilities and outright divergence of the numerical solution process.

In concluding this section we note that, in general, the set $\mathcal{T}$ of transmissivity values is usually given on a set of points scattered all over the domain Ω. This leads to the question of how to translate the scattered information about $\mathcal{T}$ to a more ordered representation along some admissible Γ curve, as required in the above solution process. The answer to this question is fairly simple. Given the fact that the characteristic curves and the general T_g solution are available to us, these scattered T values can simply be propagated, or back-projected, along their corresponding characteristic curves up to the curve Γ (see Figure 2). It follows from the definition of T_g and the expression for T in equation (3.5) that the value of transmissivity at the point of intersection, (x_0, y_0), of the characteristic curve starting from a point of measurement, (x_0', y_0'), and the curve Γ

is the ratio $T_\gamma(x_0,y_0) = T_{meas}(x_0',y_0')/T_g(x_0',y_0')$, where $T_{meas}(x_0',y_0')$ is the transmissivity measured (or otherwise assigned from 'soft data' etc.) at (x_0',y_0') belonging to the set T.

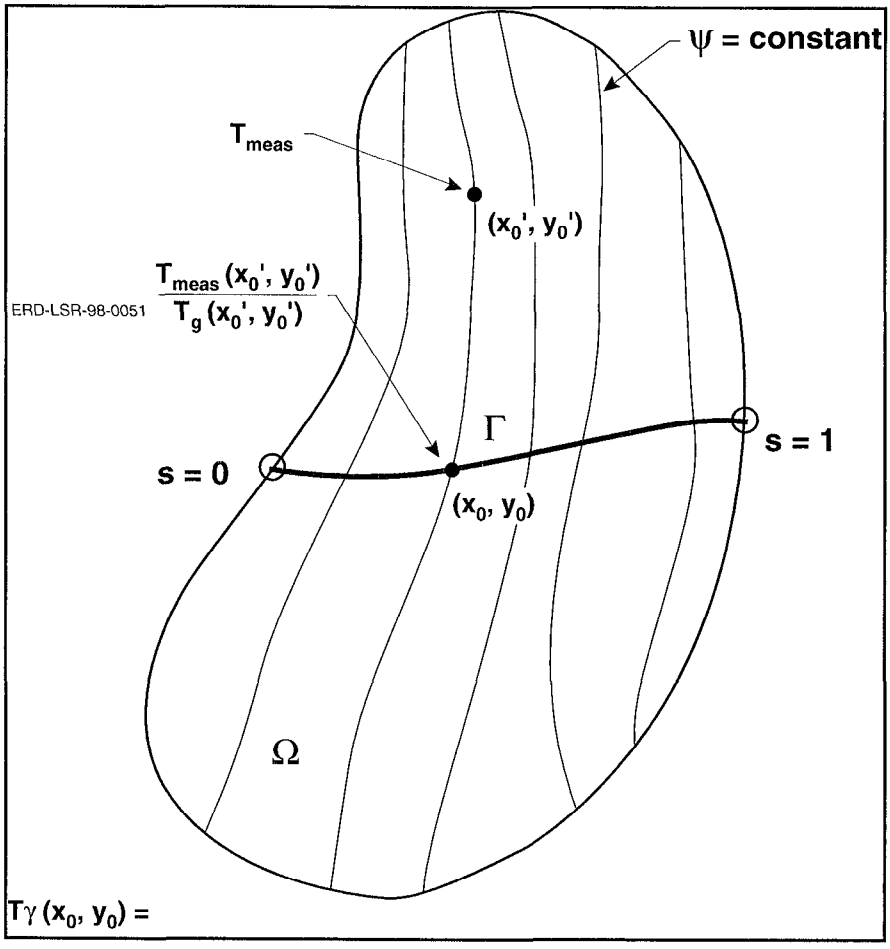

Figure 2: **Schematic representation of an admissible Γ curve in a domain Ω. Transmissivity values measured at (x_0', y_0') can be projected to the Γ curve by procedures developed in later sections of the report.**

4.0 APPLICATION AND RESULTS

This section considers three example problems, with numerous cases to illustrate specific features. Two examples were constructed with synthetic data sets and have known distributions of h and T. These examples are solved and compared with the 'true' solutions in order to better understand the capabilities and limitations of the present approach. A third example was constructed from the Livermore Site Environmental Restoration data base for the Superfund cleanup of contaminated ground water at Lawrence Livermore National Laboratory (LLNL). Extensive analysis was carried out on the synthetic cases because they enable one to verify code algorithms and logic against known solutions. They also enable one to evaluate the behavior of the method when arbitrary under-sampling conditions are imposed computationally.

The first example problem consists of a pair of compatible functions T(x,y) and h(x,y) that are analytic everywhere. In a second example problem, T is selected to be a discontinuous staircase-like function, and h is then constructed as the solution of a forward BVP with the staircase-like function T for the transmissivity. A fuller description of these simulations follows.

Example problem 1: The pair (T,h) is given by the following hyperbolic functions (see Figures 3 and 4):

$$h(x,y) = a + b\ \sinh(n\ (x^2 - y^2)) \tag{4.1a}$$

$$T(x,y) = c/\cosh(n\ (x^2 - y^2))\ \cosh(m(xy - d)). \tag{4.1b}$$

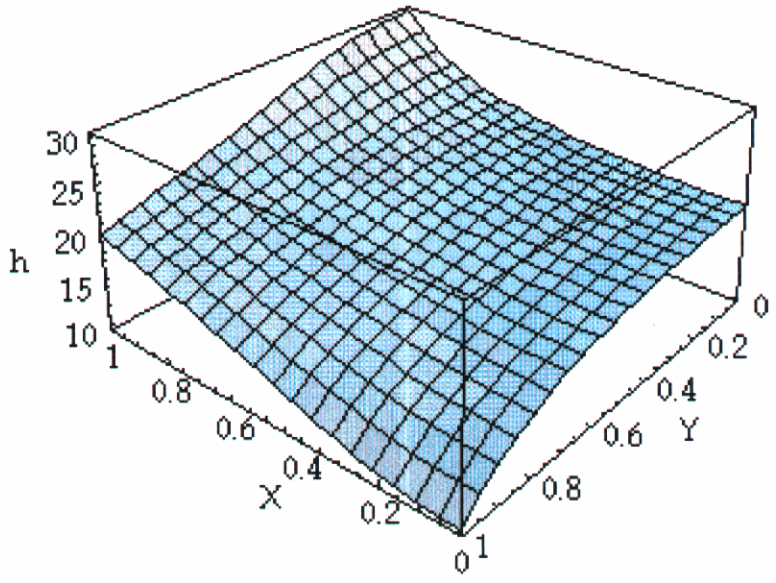

Figure 3: Plot of synthetic head h, as given by expression (4.1a) for a = 20, n = 2, and b = 10/sinh(n) in example 1.

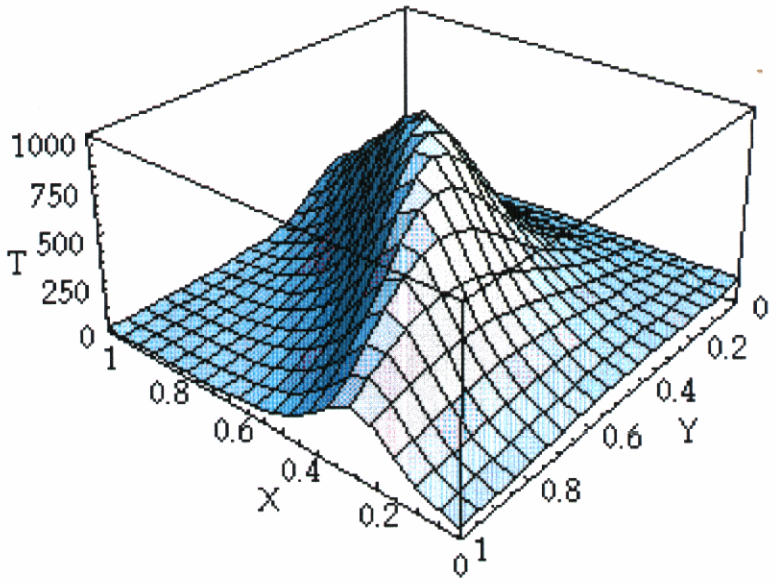

Figure 4: Plot of synthetic transmissivity T, as given by expression (4.1b) for c = 100, n = 2, m = 12 and d = 1/4 in example 1.

The domain Ω is taken as the unit square ($0 \le x \le 1$) by ($0 \le y \le 1$); and the parameters a, b, c, d, n and m are given the values 20, 10/sinh(2), 1000, 1/4, 2 and 12, respectively. This chosen set of parameter values allows h to vary from a low of 10 to a high value of 30. The corresponding limits for T are .25 and 1000, respectively.

If units of ft and ft^2/day were to be assigned to the ranges of h, 20 ft, and T, nearly 1000 ft^2/day, then these ranges would resemble those found in field measurements. It can also be noted that, besides choosing T so that it is always positive and bounded away from 0, its shape could well represent a geologic feature of say a braided-stream sand deposit embedded in a fine-grained over-bank deposit. The smooth and symmetrical shape of the function is ordinarily not a natural occurrence.

Example problem 2: A domain Ω consisting of the square ($-4 \le x \le 4$) by ($-4 \le y \le 4$) is selected. As shown in Figure 5, Ω is partitioned into 64 equal blocks, or zones, of unit squares; and T is assigned a constant value on each of these 64 zones.

The constant zonal values of T alternate several times between increasing and decreasing geometrically, giving rise to a haphazard staircase-like shape with a range of T between 1 and about 75. Given this distribution for transmissivity in Ω, the following BVP for h is solved numerically: $\nabla\bullet(T\nabla h) = 0$ in Ω, along with the BCs h = 100 on the side x = -4; h = 10 on the opposite side, x = 4, and zero flux condition along the remaining sides $y = \pm 4$. The solution to this BVP was obtained to a very high accuracy for the pair (T, h) and is shown in Figure 6 as head isocontours. This solution pair is used shortly to test the present approach for the effects of data undersampling in parameter estimation. This example is intended to be an extreme opposite to example 1.

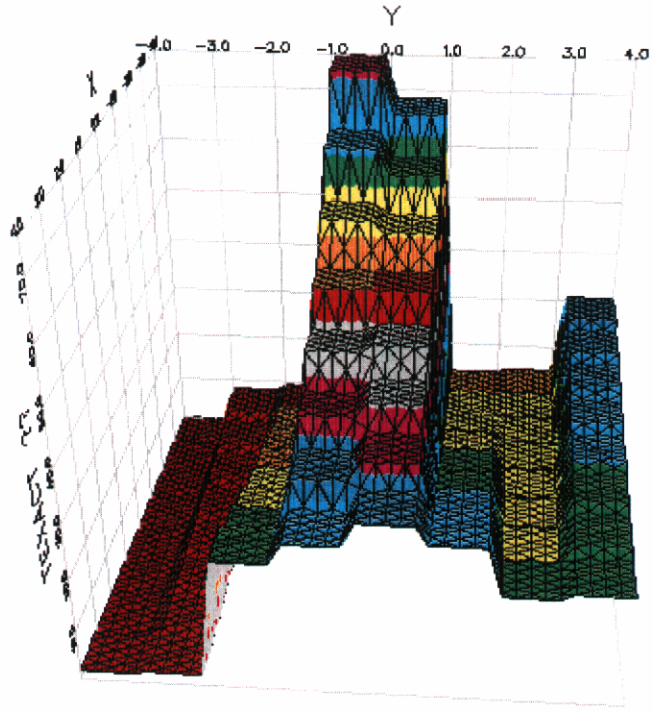

Figure 5: **Plot of synthetic transmissivity used in example 2.**

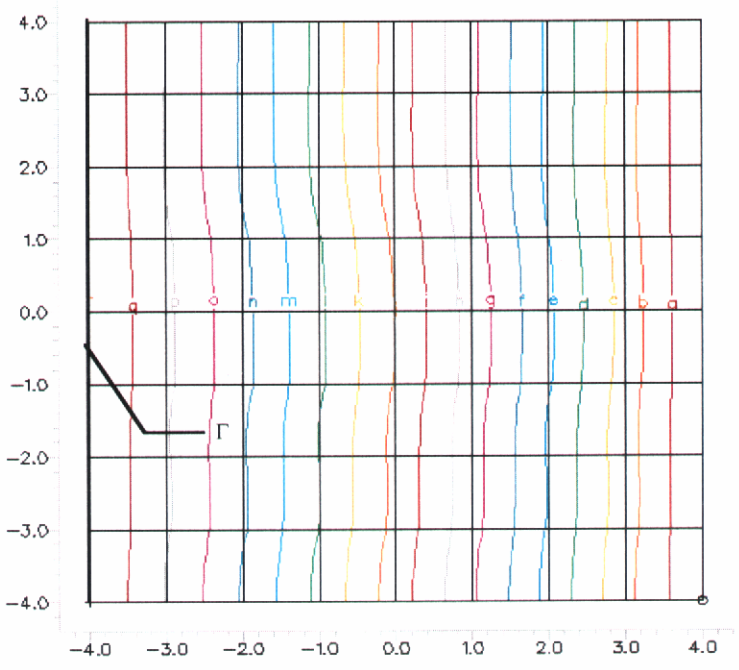

Figure 6: **Isocontour plot of the solution h(x,y) in example 2. The contours a, b..., q correspond to h = 15, 20, ..., 95 respectively.**

Example problem 3: In contrast to the previous two cases, this example employs a genuine set of measured head and transmissivity data. The data involved were collected in the month of April, 1989, and are found in the archival data base (EPD Data) of LLNL, Livermore Site, Superfund, Environmental Restoration Division. The particular choice of the month of April is favored because the recorded head data is traditionally known to be nearest to its mean seasonal values in April. Also, measurements collected during the year of 1989 were not impacted by internal sources and sinks due to remedial pumping from environmental restoration wells in the aquifer. In later years, during cleanup operations, hundreds of extraction wells were installed; and the head data were locally perturbed from ambient values. (Data as recent as February 1998 are presently available.) Hydrologically speaking, the data considered in this example are a subset corresponding to hydrostratigraphic unit 2 or HSU2, which was extracted from the original larger set (See Figures 7 and 8) (Blake *et al.*, 1995). This hydrostratigraphic unit HSU2 is the predominant contaminant bearing subsurface unit at the Livermore Site. Once more, a subset of this latter set was extracted by removing some anomalous data points for a variety of reasons such as, very close proximity of points, unrealistic values due to errors of interpretation, data base errors, etc. In all, 82 head data points remained to form the set $\mathcal{H}$ (see Figure 7), 19 of which were used to form a closed boundary that contained the remaining 63 data points. Likewise the transmissivity data used here are sampled from a larger data set that includes all the tests done in HSU2. This data was determined by using industry standard test model inversion techniques (Theis, 1935; Cooper and Jacob, 1946; Hantush and Jacob, 1955; Hantush, 1960). Quality ratings 'excellent' to 'poor' were assigned to each test. Only excellent and good values of T were used in this example problem. Median values of T were used when multiple observations were made at a single well. In all, 32 points for inferred transmissivity data were retained to form the set $\mathcal{T}$ (see Figure 8). All members of $\mathcal{T}$ and $\mathcal{H}$ are listed in Tables 1 and 2, respectively, in the Appendix, along with their corresponding (x,y) location (referred to with the state of California coordinate system) and well ID. For ease of reference, these tables retain the original ordering of entered data; but they do not list omitted values. Also note that the numerical results presented here were carried out in a domain Ω contained in the unit square (0, 1) x (0,1), which was obtained by a simple translation followed by a scaling of the axes.

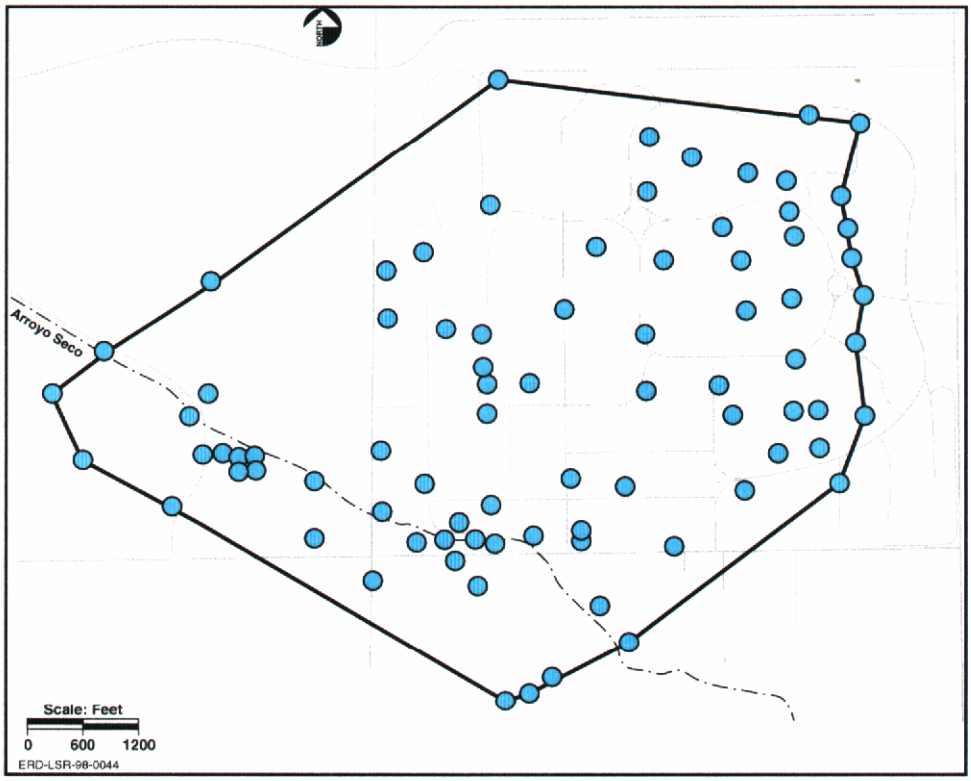

Figure 7: **Map of the LLNL, Livermore Site area. The Livermore Site is a Superfund site and is about 1 mi. square (see outline shape). Open circles (blue) are monitor wells where h has been measured monthly since 1989. This data set is from April of 1989, prior to the initiation of remediation well pumping.**

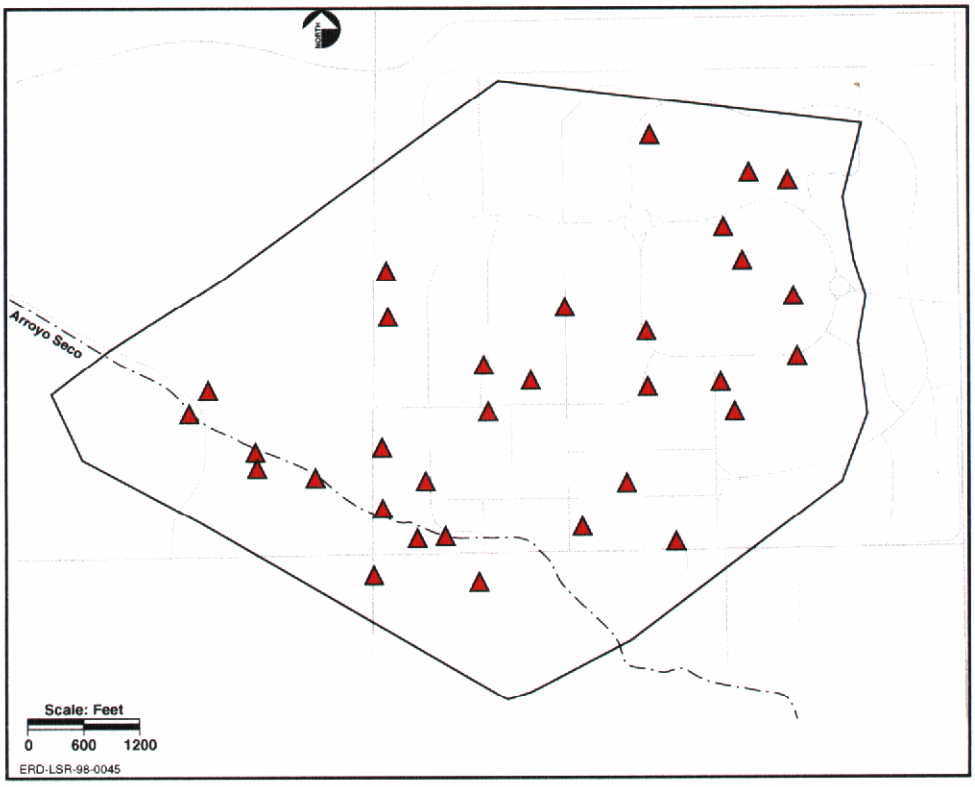

Figure 8: **Closed triangles (red) are the well locations where hydraulic tests were conducted from 1989 to present. Only the highest quality tests were used. The values range from about 20 to 6,100 ft^2/day.**

Six cases are considered to demonstrate various aspects of this parameter estimation technique. The first four cases use the analytic functions for h and T from equation (4.1). Case 5 is the second example problem with a synthetic data set for 64 discontinuous zonal transmissivities. This transmissivity model is analogous to many conceptual models that use zonal transmissivities in practical applications. Case 6 is actual field data of h and T from LLNL's ground water restoration project. This is a real test of the technique because an exact answer can never be obtained, which suggests that the answers attained will always depend on the amount, location, and distribution of available data. These various cases are discussed in greater detail in the remainder of this report.

Accuracy measures in the PDEase toolkit are controlled by a few input parameters. In addition to global error minimization, which is inherent in Galerkin methods, additional measures of local error control the unstructured grid refinement process during problem solutions. For evaluating PDE solution accuracy in our results, two different error measures for a solution f are evaluated and graphed: the maximum relative error norm MREN = max $|(f_{calc} - f_{exact})/f_{exact}|$, and the L^1 relative error norm, or average relative error (ARE), defined by

$$ARE = \iint_{\Omega} |(f_{calc} - f_{exact})/f_{exact}|\,dA. \qquad (4.2)$$

With the exception of nonlinear problems, all initial trial solutions required by the conjugate gradient methods in the PDE solver were arbitrarily chosen to be 1. An orthomin norm (Jea and Young, 1983) conjugate gradient method is used in the toolkit for symmetric differential operators and a Lanczos/orthomin biconjugate method is applied for asymmetric operators. A normalized CG method due to Vandenberg (1988) was incorporated in the toolkit for solution of highly asymmetric problems.

Synthetic Examples. Cases 1 and 2: Verification of purely forward and inverse solution techniques

Two cases are verified using the analytic functions in equation (4.1). In Case 1 exact values are known for T in Ω and for h $\partial\Omega$. The forward problem is solved for h. In Case 2 exact values are known for h everywhere and T is given only on Γ. These two cases are a test of the numerical proficiency of the adaptive Galerkin techniques employed by PDEase on the forward and inverse aspects of the problem independently. Traditionally, fixed numerical grid methods are employed to solve these PDE problems; they are known to generate numerical errors that would be problematic in the present work.

Case 1 Results: The exact and the numerical solution obtained are virtually indistinguishable. Calculated head isocontours are shown in Figure 9. These results demonstrate that, given a true BVP, the dynamic adaptive grid Galerkin technique employed in PDEase is capable of calculating h everywhere in Ω to a very high accuracy. For a PDE error criteria (used in PDEase) of 1.E-6 the resulting errors in the h solution were MREN < 0.1% and ARE < 0.01%.

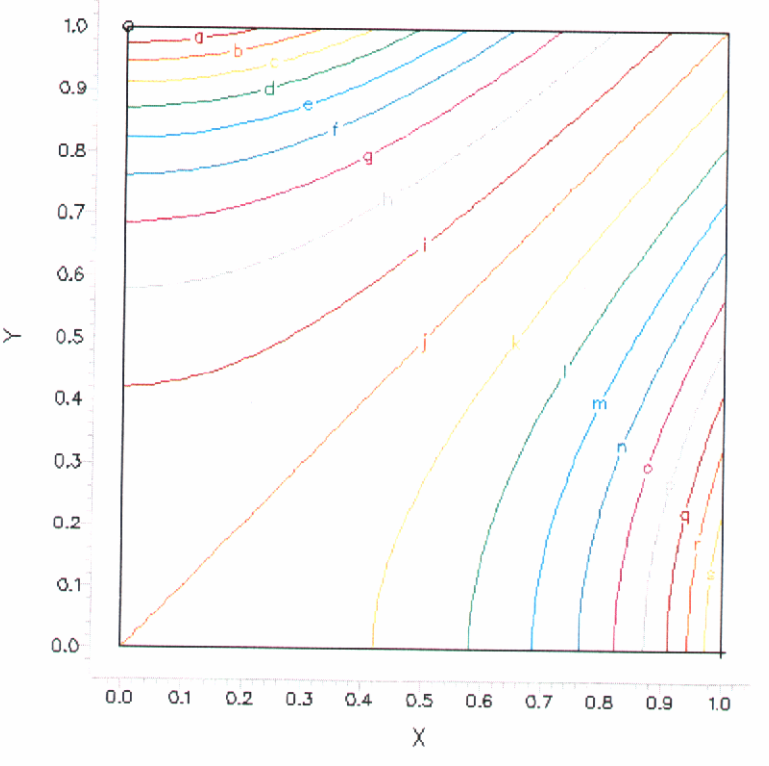

Figure 9: Isocontours of h in Case 1. MREN < 0.1% and ARE < 0.01%.

Figure 10 shows the adaptive grid configuration, which contained 4800 cells (triangles), at the conclusion of this problem's execution. At the start of the problem, there were approximately 100 cells in the initial grid that was constructed automatically by the toolkit.

Case 2a: Solve the pure inverse problem for T where transmissivity is given by equation (4.1b) along Γ, chosen here to be the 45-degree diagonal. This case seeks to verify the following proposition: A parameter estimation method that is expected to solve real-world problems with undersampled data, where a 'true solution' can never be known, should also be expected to solve a well-posed problem for unique T(x,y) when given a 'perfect' data set for h on Ω and T on Γ.

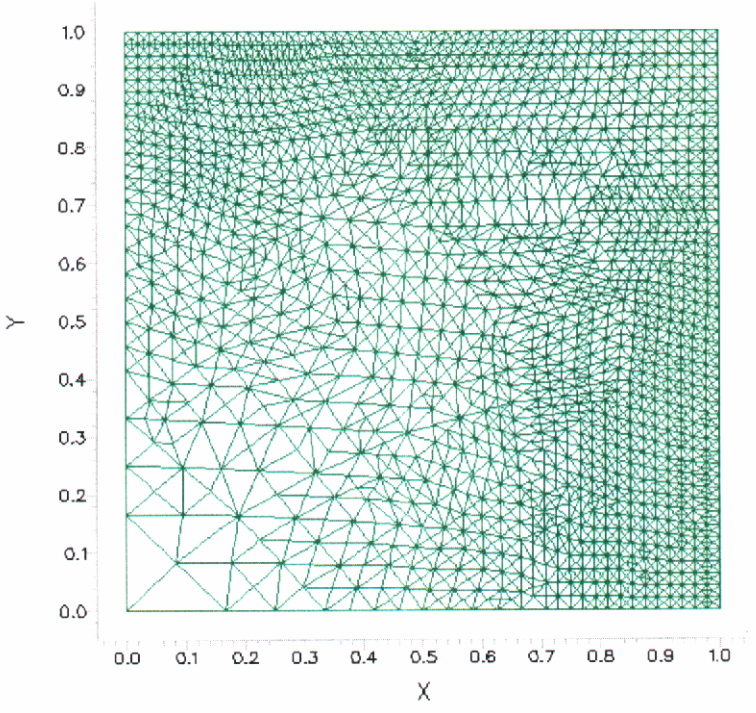

Figure 10: The grid at conclusion of the case 1 solution has 4,800 individual cells. The density of cells highlights regions in Ω, where the technique had to subdivide in order to meet the local error criterion.

The calculated results (Figure 11) demonstrate that, the PDEase solution techniques are capable of calculating the solution to any desirable accuracy within practical limits. The final grid in this case incorporated over 7,600 cells and demonstrated the difficulty of accurate numerical integrations of the PDE in regions of Ω where transmissivity gradients are large. The adaptive solver is essential in solving this type of problem, where the gradients of T in nature can be highly disparate.

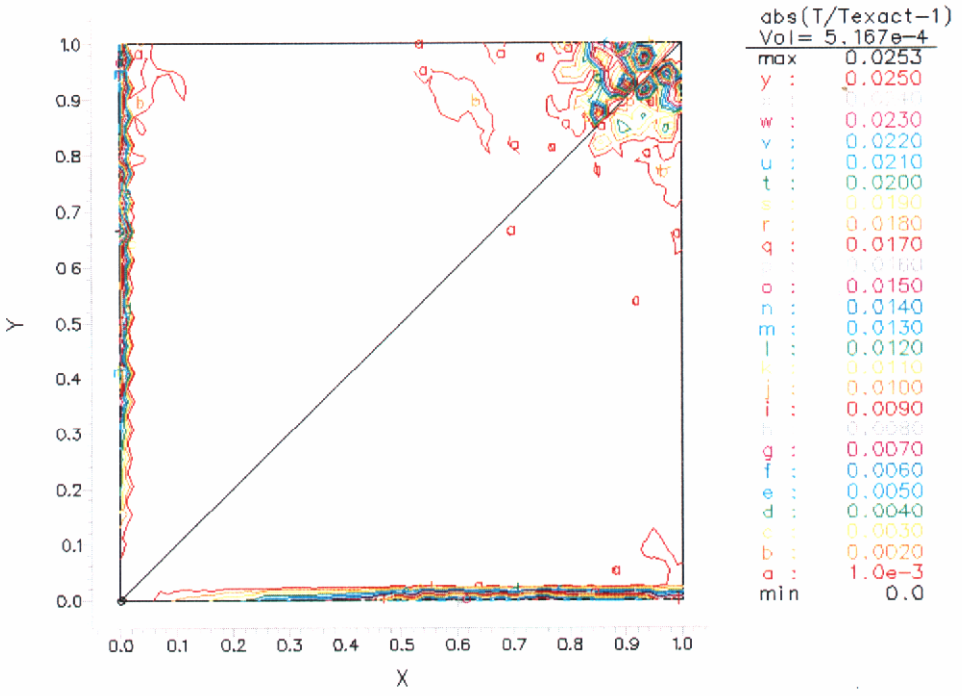

Figure 11: Contour plot of absolutely relative error in Case 2a. MREN < 2.5% and ARE < 0.05%.

The maximum relative error is < 2.5%, and the ARE is < 0.05% (see Figure 11). The relative error is maximum along the left and bottom boundaries, which together form a degenerate characteristic curve. Also, Figure 11 shows an area in the neighborhood of (1,1) with significant relative cell error. Errors in this neighborhood are due to the diminishing values of T there, which in turn cause larger absolute relative errors.

Case 2b: Solve the pure inverse problem for T, where transmissivity is known only on Γ, which is now taken as the side boundary $x = 1$ and $0 \leq y \leq 1$. It is expected that the solution in this case will be degraded only slightly relative to the previous Case 2a, where the T information given on Γ propagated equally about the diagonal. In contrast, the information along Γ in Case 2b is propagated twice as far as before and is thus subjected to more degradation as it traverses the domain along the characteristic curves. The fact that the head gradient vanishes at (0,0) is likely to contribute to the increase in relative error that is seen in this region.

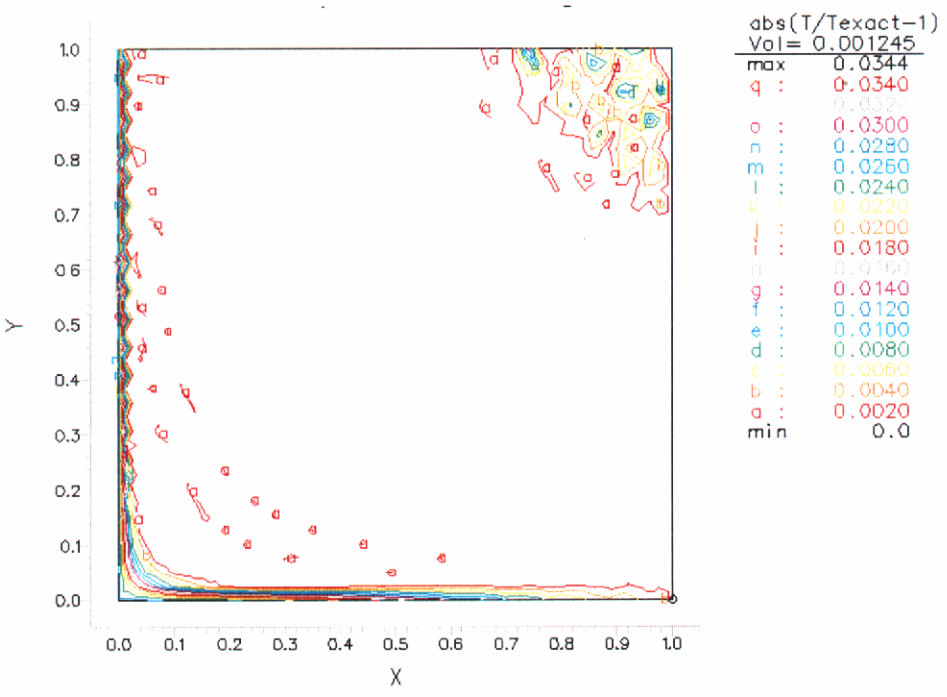

Figure 12: Contour plot of absolute relative error. MREN < 3.5% and ARE < 0.08%. The choice of Γ is significant but not critical in this synthetic example.

Case 2c: Solve the transmissivity problem as posed in Case 2b with the factorization method described by equations (3.16)–(3.18), using $T_g = 1$ on Γ. The results are presented for the component factors Φ and T_g in Figures 13 and 14 and for T_{calc} in Figure 15. The results for T_{calc} are visually indistinguishable from the analytic solution in equation (4.1b) and Figure 4. The errors in the calculated transmissivity are MREN < 3.5% and ARE < 0.08%. As in previous cases, the maximum errors occur near degenerate streamlines along the left and bottom axes and where very small values of T occur near (1,1).

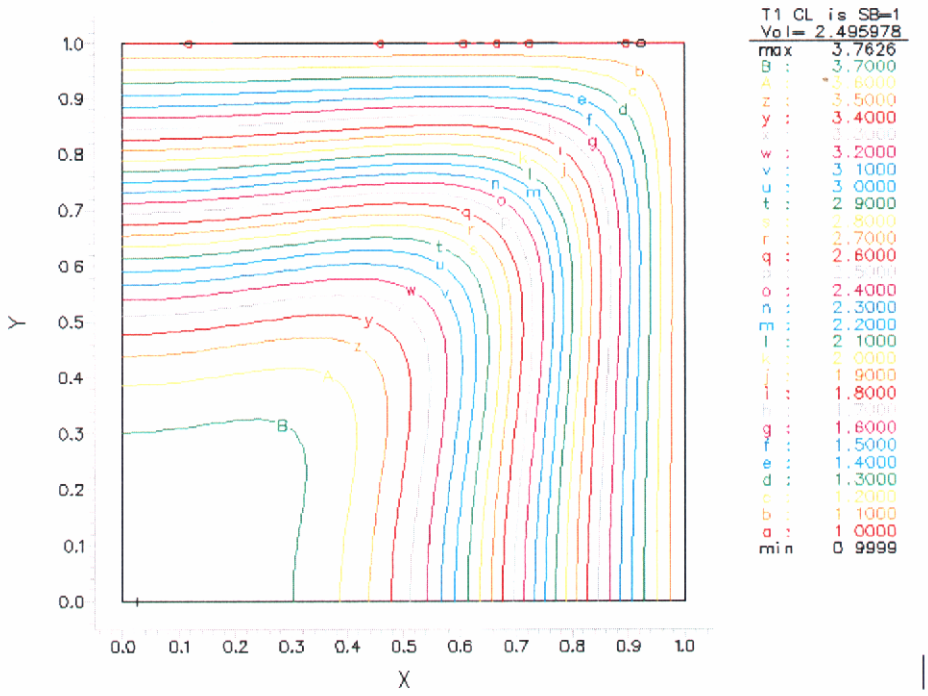

Figure 13: Isocontours of T_g , for case 2c. Values of Tg range from 1.0 along the curve Γ to 3.76 at the origin.

The T_g surface shown in Figure 13 has the shape of a plateau with a ridge oriented along Γ from (0,0) to (1,1). A possible interpretation of this surface is that T_g reflects the information contained in the h data about transmissivity when very little is known about T. The Φ solution is shown in Figure 15. The Φ surface evidently parallels the streamline function. The intersection of Φ with Γ coincides with the maximum ridge in the T_g surface (Figure 13) and takes the appropriate value of T_g in order to reproduce the maximum value of T of 1,000 shown in Figure 4.

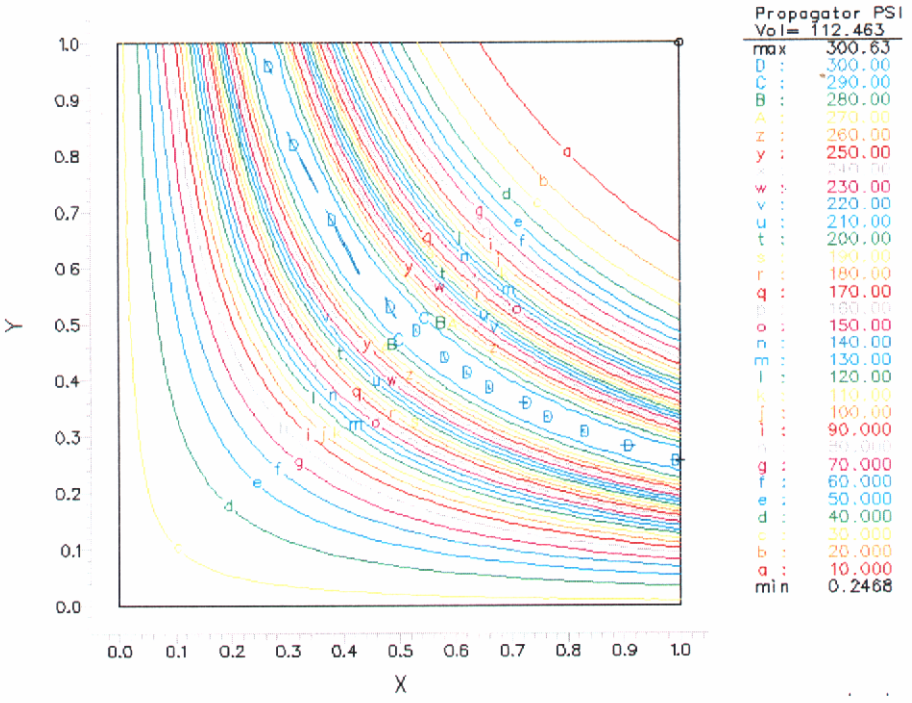

Figure 14: **Calculated particular solution, Φ, for case 2c. Values of Φ range from .25 to 300 in this example. The similarity of the Φ isocontours to the original T function in Figure 4 is evident.**

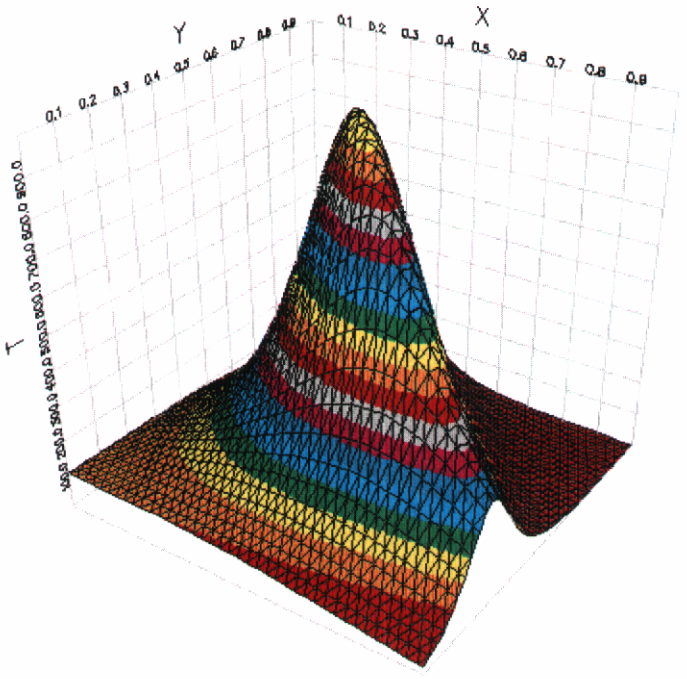

Figure 15: **T_{calc} for case 2c from the multiplication of T_g and Φ. This result is visually indistinguishable from the original T function shown in Figure 4.**

Synthetic Examples. Case 3: Analyze undersampling in head data from example problem 1.

Case 3: The analytic or numerical solutions from problem 1 can now be sampled with varying degrees of sparsity in order to obtain an undersampled data set for a new problem that resembles the practical circumstances that are encountered in the field. Figure 16 depicts head measurement locations in an undersampled data set with 81 h 'measurements' given at ((i-1)/8, (j-1)/8; i, j = 1, ..., 9. Transmissivity is given along the curve Γ, which is taken here to be the 45° diagonal. Head values were linearly interpolated between the data points on $\partial\Omega$. Using the full, factorized parameter estimation approach described with equations (3.16)–(3.18), the results retained much of the essential character of the original problem (Figures 3 and 4). The MREN < 40% for transmissivity occurred along the axes, as shown in Figure 17, and is less that 2% on the interior. The ARE < 3.2%.

Spatial filtering of the head gradients in equations (3.17b and c) was crucial for attaining these error levels. (Without filtering, numerical gradients can be very unstable and seriously degrade parameter estimates.) That maximum errors occurred near the axis is probably attributable in part to the fact that errors/noise in head gradients are largest near boundaries where there is little support. This factor may further suggest practical considerations of the relative worth of measurements at boundaries versus interior points. To gain a sense of the significance of interpolation errors at $\partial\Omega$, this problem was solved using the 'true' head values on $\partial\Omega$ with a 7x7 stencil of interior data points. We found that the MREN dropped to 19% and ARE < 2.2%, supporting the above suggestions.

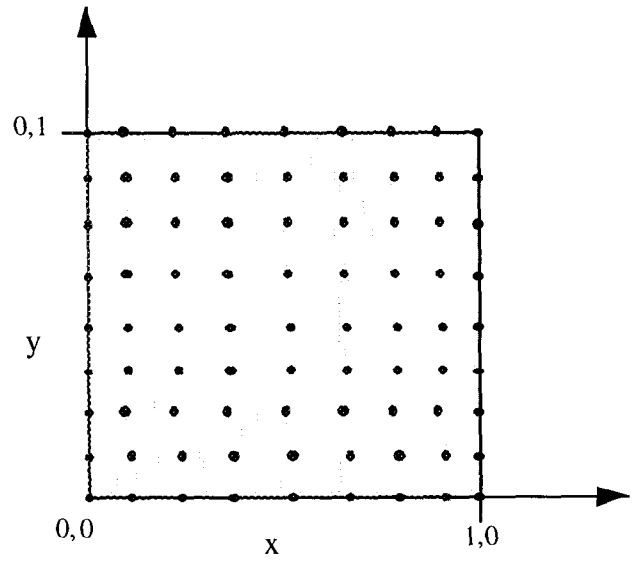

Figure 16: Schematic representation of case 3. The data set from h solutions in example 1 (Figures 3 and 4) was sampled at 81 discrete points including the boundary. Boundary h values are linearly interpolated along the boundary. T is known only on Γ along the 45° diagonal.

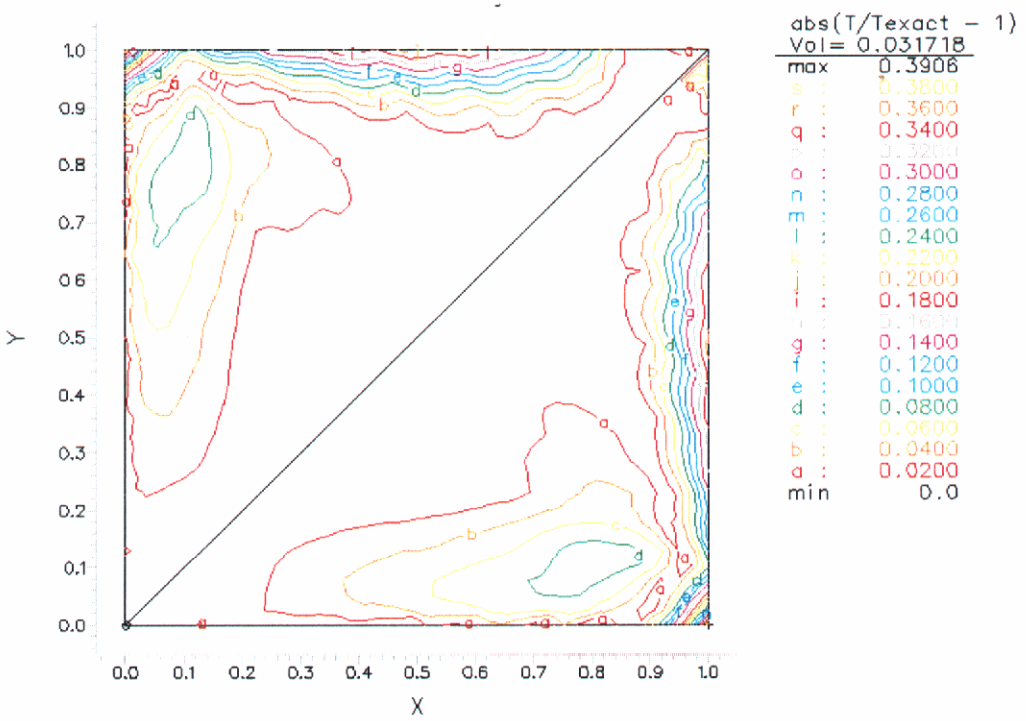

Figure 17: Error isocontours for the 9x9 undersampled h problem. Maximum error occurs on the edges along the axes and does not exceed 40%. However, the average relative error is < 3.2%.

Synthetic Examples. Case 4: Undersampling in head and transmissivity data for example problem 1.

Case 4: Solve the (9x9) undersampled data set considered above, but with transmissivity values at the 49 interior locations ((i-1)/8, (j-1)/8; i, j = 2, ..., 8 and at the corners (0,0) and (1,1). This is the general situation that is encountered in the field, except that a 'true solution' is available in the present instance. As in the previous case, the given 32 head values on $\partial\Omega$ were linearly interpolated to construct the boundary data for h. The 45° diagonal was selected as Γ, and all the 51 given transmissivity values ('measured data') were back-projected along characteristics onto Γ, with T_γ being evaluated on Γ as described previously. But what to do about values of T_γ between the discrete points that were projected from T_{meas}? Several alternatives are possible: (i) interpolate (or extrapolate) between 'measured' T_γ values along Γ, (ii) use additional soft-data (including human judgment for transmissivity to generate additional T_γ, (iii) or use other techniques (e.g., stochastic models) to generate additional T_γ prior to interpolations and/or spatial filtering of T_γ along Γ. In the present example, the T_γ values were declustered, interpolated, and smoothed by spatial filtering analogous to u and v. Figure 18 plots the T_γ (red curve) projected from the discrete datum points on the same graph as the 'true' T_γ used in problem 1. The errors in the calculated transmissivity (Figure 19) were MREN < 136% and ARE < 8% (Figure 19). When testing the significance of not having 'measured' T data at the extremity of Γ in the corners (0,0) and (1,1), we found that MREN ≈ 2500% at those corners and ARE < 11%. This result raises significant questions regarding the relative worth of various data types, locations, and information content when designing field measurement strategies for effective subsurface characterizations.

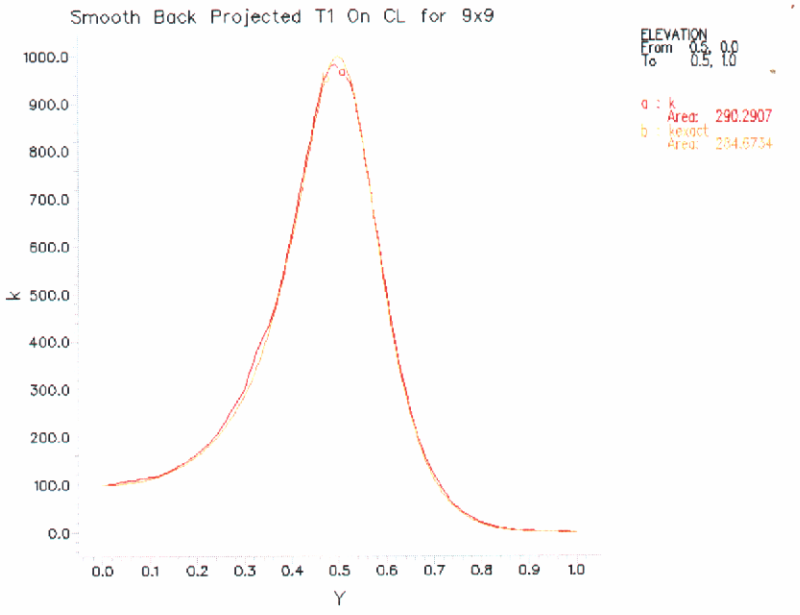

Figure 18: **Plot of smoothed T_γ (red curve) that was back-projected from undersampled h and T data and also the 'true' T_γ (orange). Maximum error < 1%.**

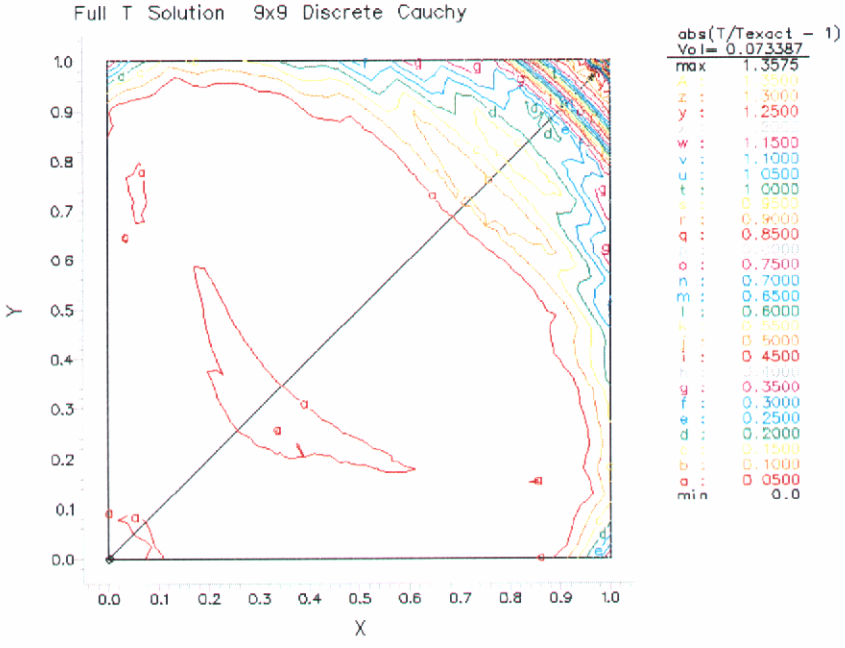

Figure 19: **Plot of MREN for the undersampled h and T problem in case 4. Maximum error occurs in the corner of Ω where T is small. MREN < 136% and ARE < 8%.**

Synthetic Examples. Case 5: Undersampling in head and transmissivity data from example problem 2.

Case 5: Solve transmissivity with undersampled data from problem 2 (Figure 5). 'Measured' h data are given at the center of each of the 64 blocks (shown in Figure 5), and T is given along the side x = -4; ($-4 \le y \le 4$). Exact transmissivity values were assigned along Γ in the calculation of the particular solution Φ equation (3.17). Using the factorized methods described previously, the discontinuous transmissivity features of the 'true' solution (Figure 5) are resolved as shown in Figure 20 for T_g and in Figure 21 for T_{calc}. As expected, sharp discontinuities in T are smoothed by the undersampling. The general features have however been reproduced with surprisingly good fidelity from the information contained in such few observation points, in our opinion. The MREN < 245% and ARE < 19%. Maximum errors, as seen in Figure 22, occur at the T discontinuities, as anticipated. It is here that adaptive grid PDE solvers apparently demonstrate their worth for calculating gradients with the maximum fidelity that is compatible with supporting measured data.

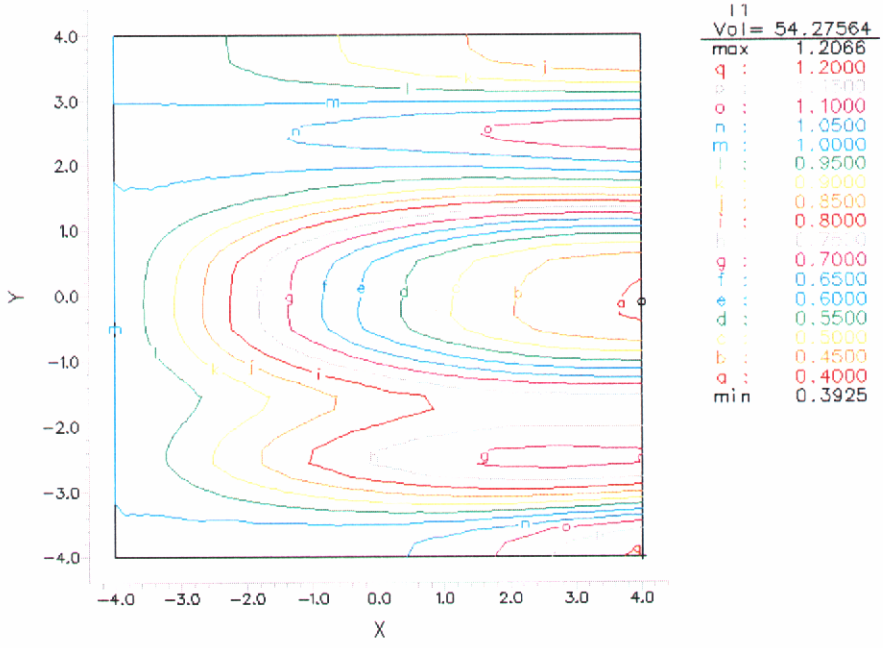

Figure 20: Isocontour of T_g for case 5 with $T_g = 1$ along Γ.

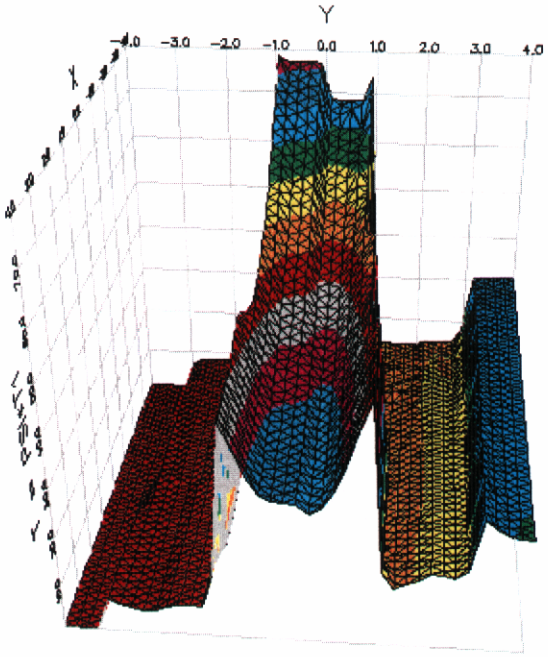

Figure 21: T_{calc} **for case 5. This estimated transmissivity has the overall shape of the 'true' solution shown in Figure 5.**

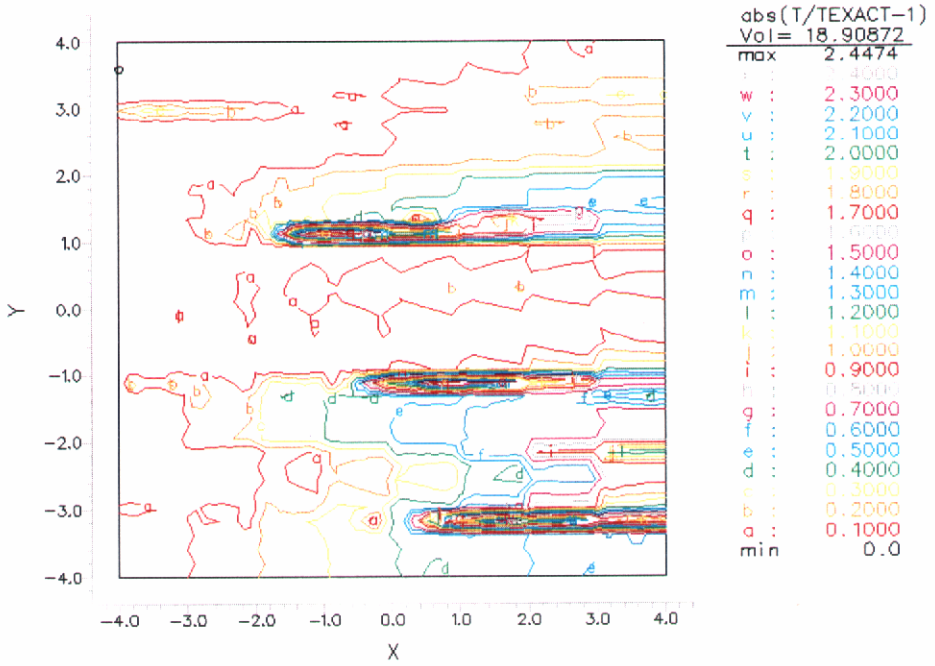

Figure 22: **Plot of MREN for the undersampled h and T problem in case 5. Maximum error occurs along horizontal lines between large changes in T and does not exceed 245%. The ARE is <19%.**

LLNL HSU2 data set, undersampling in both head and transmissivity data for example problem 3

Case 6: Estimate lateral transmissivity distribution in HSU2 using the LLNL, Livermore Site, head data from April 1989 and T data from 1989 to present. (It is reasonable to assume that the aquifer thickness is known and the transmissivity is a function of only rock properties in the saturated porous medium at LLNL). In the present case, the true transmissivity is unknown; and professional judgment is used to select the smoothing parameters. A slightly non-convex domain was constructed from this data set and is displayed in Figure 7. Transmissivity was determined using standard analysis of pumping tests in wells, with test durations ranging from 4 to 72 hours and with wide variations in quality. Taking into consideration all relevant aquifer information, a data quality value was assigned for each test result. Only 'excellent' and 'good' measurements were used in this analysis. In some well locations, several T estimates have been made over the years and vary in value. In such cases the median values were selected. The effect of data uncertainties will be considered in multiple realizations in conjunction with sensitivity analyses in future work. Applying the criteria indicated above, the retained T data set is displayed in Figure 8. The original estimates for T accounted for the thickness of HSU2. The estimates for T range from 15 to 6370 ft^2/day.

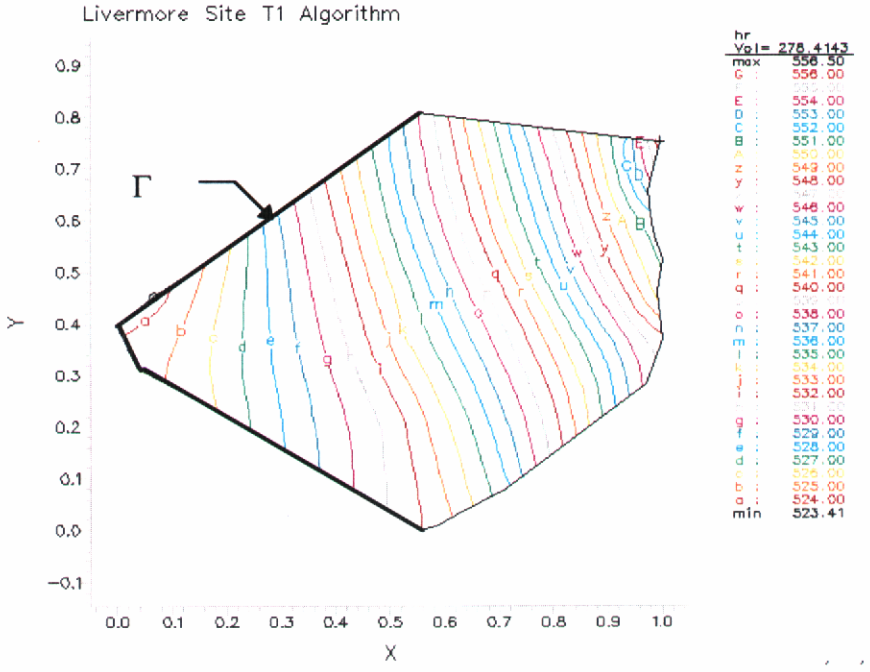

Figure 23: **Plot of head isocontours for h_r in step 1 for the LLNL/HSU2 domain. Head values range from 558.5 ft in the northeast to 523.4 ft in the west.**

Assuming T = 1 throughout the domain, a preliminary estimate of head isocontours (Figure 23) and characteristic map were calculated in order to select Γ. The characteristic map calculated with equation (3.11) is shown in Figure 24. The western boundary was selected as Γ and is highlighted on Figure 23. Values of h measured in the domain range from 558.5 ft in the northeast to 523.4 ft

in the west. In step 2, the smoothing of h_r produced h_s values that matched measured h values at observation points to within 0.5 ft (consistent with measurement errors). T_g was calculated with different values for the gradient smoothing parameter α and the regularization parameter ε.

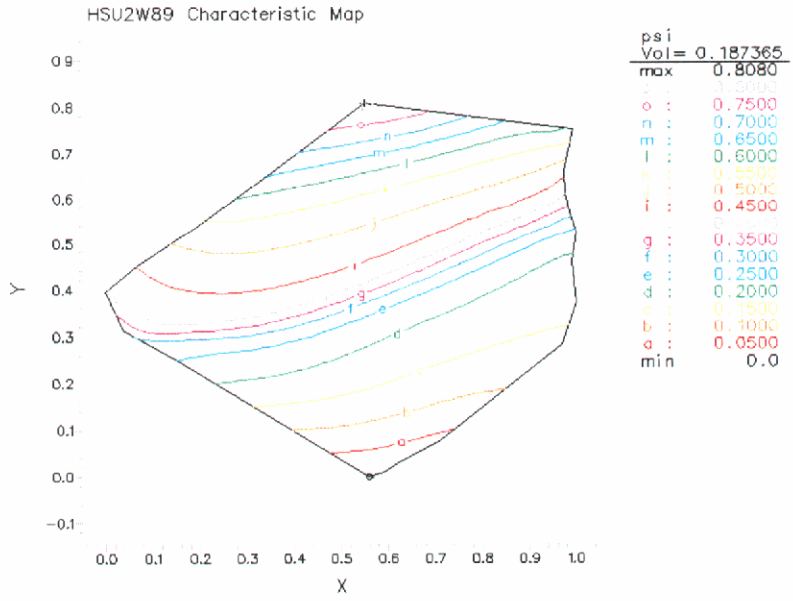

Figure 24: Map of characteristics (equation 3.11) emanating from Γ, which is parameterized by the independent variable y. (See Figure 23 for Γ location.) These characteristics correspond to the final calculated head distribution.

Spatially filtered head gradients were somewhat sensitive to boundary conditions, consistent with previous discussion. To examine the effect of that sensitivity, two solutions of T_g are plotted in Figures 25a and 25b for more- and less-smoothed head gradients, respectively. The same general information content is apparent in T_g and thus T_{calc} for both head gradient representations. A rigorous quantitative rationale for this spatial filtering in the general non-linear systems solved here has not yet been developed.

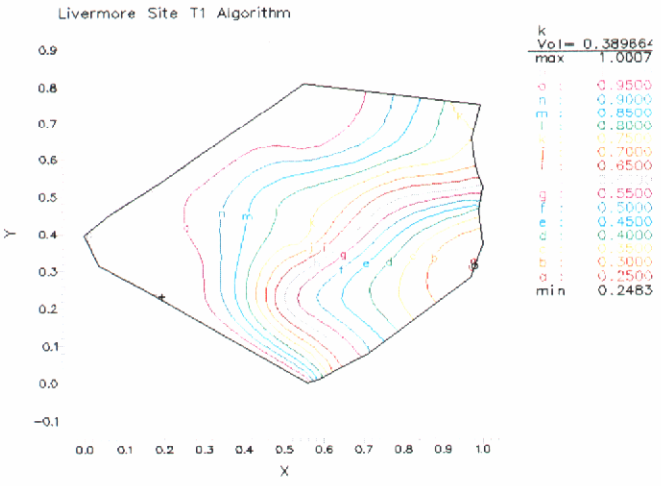

(a) more-smooth head gradients

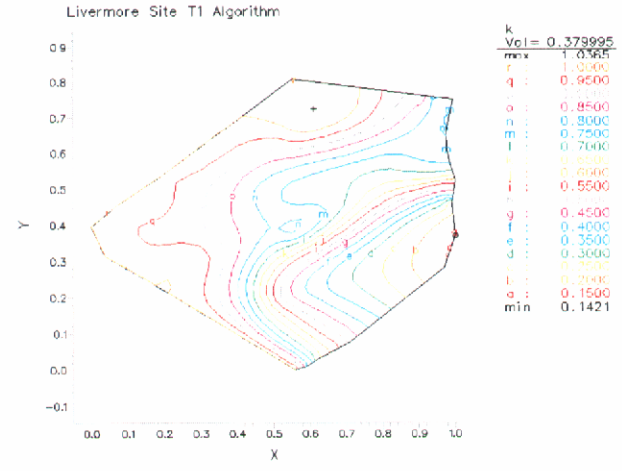

(b) less-smooth head gradients

Figure 25 : T_g is plotted for two degrees of head gradient smoothing The dynamic range of the values for T_g is greater for the less-smoothed solution relative to the more-smoothed version (approximately 50%). The general structure of T is similar in both versions.

All 'measured' transmissivities are projected along the characteristics (Figure 24) parametrized by y to Γ (see Figure 26). Large variations in the T_γ on Γ occur over short spatial intervals. A simple interpolation and smoothing procedure was employed and different degrees of smoothing were examined. Each T_γ thus produced represents a potentially valid realization with varying degrees of matching to the original transmissivity measurements and to any other 'soft data' that may be brought to bear. The 2-D lateral transmissivity calculated for HSU2 at LLNL's Livermore Site (with no additional soft data applied) with smoothed T_γ (in Figure 26) is presented in Figure 27.

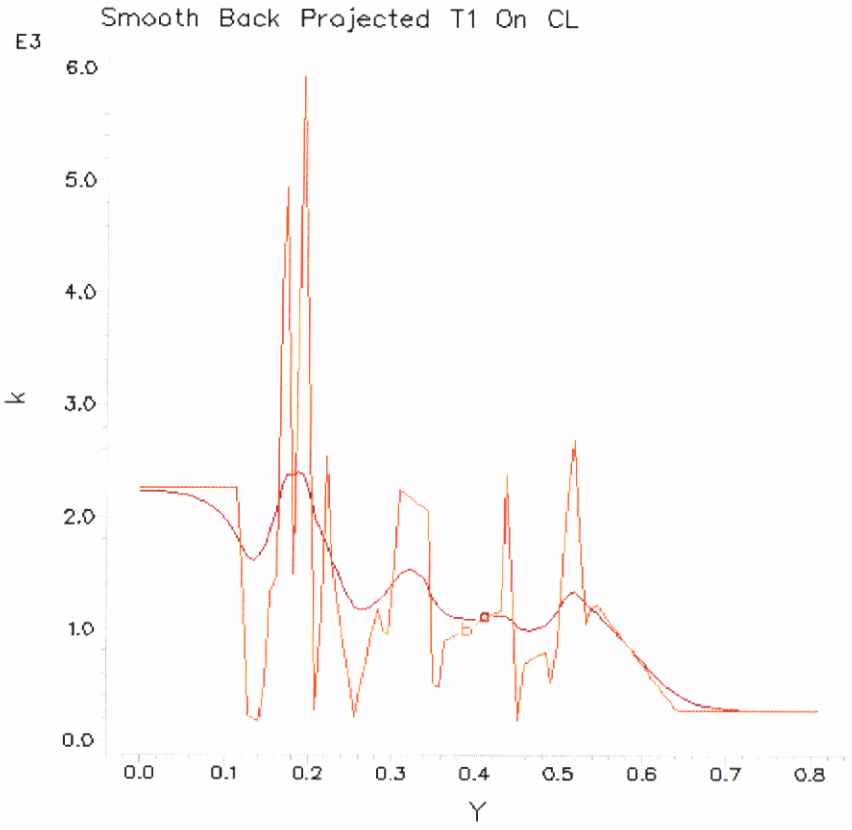

Figure 26: **Calculated T_γ versus distance along Γ for all transmissivities projected from measurement locations (curve a) and linearly interpolated between intersection points on Γ. Curve a is a smoothed version of the data on Γ, which is used in the final T estimate.**

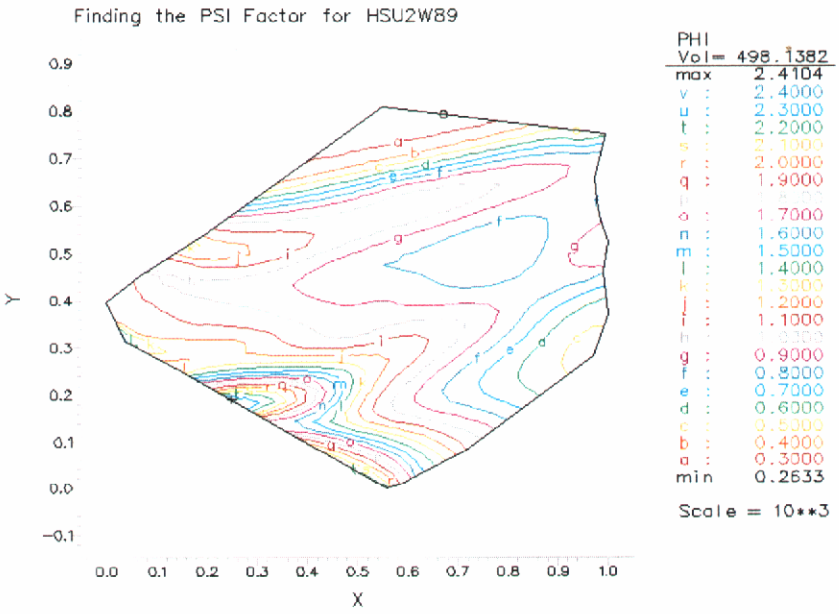

Figure 27: Estimated transmissivity for HSU2 at LLNL's Livermore Site, using smoothed versions of Tγ and T_g.

5.0 CONCLUDING REMARKS

We have seen in the foregoing text that subsurface parameter estimation techniques have two general modes of application and that basic signal processing techniques are essential for successful outcomes in each. In the first mode, sparse data is interpreted at face value. That is, the scale of spatial resolution attained in coupled estimates of transmissivity and interpolated head distributions turns out to be whatever scale is supported by the sampling of subsurface data. Since subsurface measurements are always sparse, the extent of smoothing may be greater than desired, or hoped for, in specific applications; and well-known aliasing effects of coarse-sampling are unavoidable (see Bracewell, 1986, and McGillem and Cooper, 1984). Aliasing effects occur when information that has high spatial frequency components in the actual physical system is observed via a band-limited function derived from coarse sampling. As noted by Bracewell (1986), high-frequency signal components shift down and 'masquerade' at low frequencies inside the band limits of the coarse sampling function. When this high frequency tail is not too important, coarse sampling can give reasonable results in estimated parameter distributions. When that is not the case, high-frequency information can neither be retrieved nor created reliably from the physical system without finer sampling. It is here that the second mode of parameter estimation comes into play, as either an alternative to additional sampling or perhaps as support for new sampling proposals. In this second mode of application, hypothetical transmissivities are fabricated (non-uniquely) to contain high-frequency components from finely sampled simulated 'data'; and the created transmissivity realizations are then calibrated to the existing hydraulic data with forward model calculations. With the methods developed in this project, such transmissivities with surrogate high-frequency components would be additionally constrained to respect both existing hydraulic measurements of head and transmissivity and the coupled forward and inverse PDEs of kinetic physics, as described previously. But the amount of additional head data that would be required from the actual physical system in order to 'support' such hypothetical transmissivities is

generally unknown. Nonetheless, multiple realizations of surrogate transmissivities may then be processed by various formal or informal techniques in order to posit 'best solutions'. We have found that, if the first mode of parameter estimation application cannot be executed appropriately for sparse measured data, the second mode of application which attempts to generate hypothetical transmissivities with unmeasured high-frequency components becomes all the more problematic. The present project has thus focused initially on advancement of the first mode of applications, while also developing advanced tools and scientific techniques for extended investigations of sub-scale physical properties in future work.

In summary, this project has created and applied new computational physics tools and techniques for practical application in both existing and newly advanced parameter estimation methods. The objective in these broadened parameter estimation techniques is to produce model calibrations and interpolations of hydraulic head and transmissivity data for flow in porous media, subject to multiple constraints that help to mitigate adverse effects of non-uniqueness. Such data-calibrated estimations must respect not only all pertinent physical observations but also the forward and inverse PDEs that govern physical and mathematical continuity. They should additionally minimize ad hoc or purely statistical interpolations that are not themselves solutions of the governing kinetic PDEs. And they should apply signal processing techniques that can mine maximum information content from sparse, noisy data consistently with data sampling principles in non-linear systems. Many technical questions, issues, and directions for additional research have of course been left open in the conduct of this project. We believe however that the ambitious objectives set out initially have been achieved, and surpassed. Ensuing developments over time, which would build upon both the scientific formulations and the computational physics tools and paradigms incorporated in this research, will provide the ultimate judgement of that belief.

ACKNOWLEDGMENTS

The authors wish to acknowledge the LLNL Lab Directed Research and Development (LDRD) Program for supporting and funding this work and express our appreciation to the Management of the LLNL Environmental Restoration Division and the Management of the LLNL Environmental Protection Department for continued support and encouragement throughout the entire enterprise. In particular, we wish to thank Ellen Raber, Lynn Cleland, Rokaya Al-Ayat, John Kneczovich, Dennis Fisher and Bill McConachie for their advocacy and Professors Jacob Bear, David Dougherty, T.N. Narisimhan, and Lynn Gelhar for illuminating and invaluable discussions.

REFERENCES

Akcasu, A.Z., and R.K. Osborn (1966), "Application of Langevin's Technique to Space and Energy Dependent Noise Analysis," *Nucl. Sci. Eng.*, **26**, pp. 14-25.

Backstrom, G. (1994), *Fields of Physics on the PC by Finite Element Analysis*, Student Litteratur (ISBN 91-44-48671-5), Lund, Sweden or Chartwell Bratt Ltd., (ISBN 0-86238-382-X) British Library Catalog.

Backstrom, G. (1998), *Fields of Physics by the Finite Element Method—An Introduction*, Student Litteratur ab (ISBN 91-44-00655-1) Box 141, SE22100, Lund, Sweden.

Blake, R.G., M.P. Maley, and C.M. Noyes (1995), *Hydrostratigraphic Analysis: The Key to Cost-Effective Ground Water Cleanup at LLNL*, Lawrence Livermore National Laboratory, Livermore, CA., UCRL-JC-120614.

Bracewell, R.N. (1986), *The Fourier Transform and Its Applications*, Second Ed., Revised, McGraw-Hill, New York, NY.

Carle, S.F. (1996), *A Transition Probability-Based Approach to Geostatistical Characterization of Hydrostratigraphic Architecture*, Ph.D. Dissertation, Hydrology Program, Department of Land, Air, and Water Resources, University of California, Davis, CA.

Carles, S.F., and G.E. Fogg (1996), Transition Probability-Based Indicator Geostatistics: Math. Geology, **28**(4), pp. 453-477.

Carrera, J., and S.P. Neuman (1986a), "Estimation of Aquifer Parameters Under Transient and Steady State Conditions, 1, Maximum Likelihood Method Incorporating Prior Information," *Water Resour. Res.*, **22**(2), pp. 199-210.

Carrera, J., and S.P. Neuman (1986b), "Estimation of Aquifer Parameters Under Transient and Steady State Conditions, 2, Uniqueness, Stability, and Solution Algorithms," *Water Resour. Res.*, **22**(2), pp. 211-227.

Clifton, P.M, and S.P. Neuman (1982), "Effects of Kriging and Inverse Modeling on Conditional Simulation of the Avra Valley Aquifer in Southern Arizona," *Water Resour. Res.*, **18**, pp. 1215-1234.

Cooper, H.H., and C.E. Jacob (1946), "A Generalized Graphical Method of Evaluating Formation Constants and Summarizing Well Field History," *Am. Geophys. Union Trans.* **27**, pp. 526-534.

Courant D., and D. Hilbert (1953), *Methods of Mathematical Physics*, Interscience, New York, NY.

Dagan, G. (1989), *Flow and Transport in Porous Formations*, Springer-Verlag, New York, NY.

Datta-Gupta, A., D.M. Vasco, and J.C.S. Long (1997), "On the Sensitivity and Spatial Resolution of Transient Pressure and Tracer Data for Heterogeneity Characterization," *SPE Formulation Evaluation*, June, pp. 137-144.

Doherty, J. (1990), "Manual for the MODINV Suite of Software for MODFLOW Parameter Optimization," Australian Centre for Tropical Freshwater Research, James Cook University, Townsville, Queensland. 4811, Australia.

Emsellem, Y., and G. deMarsily (1971), "An Automatic Solution for the Inverse Problem," *Water Resour. Res.*, **7**(5), pp. 1264-1283.

Frind, E.O., and G.F. Pinder (1973), "Galerkin Solution of the Inverse Problem for Aquifer Transmissivity," *Water Resour. Res.*, **9**(5), pp. 1397-1409.

Gelhar, L.W. (1993), *Stoschastic Subsurface Hydrology*, Prentice-Hall, Englewood Cliffs, NJ.

Gelinas, R.J. (1976), "Comments on the Foundations of Fluctuations in Reactive Systems," *Combustion Sci. and Technol.*, **13**, pp. 269-275.

Gelinas, R.J., and R.K. Osborn (1966), "Reactor Noise Analysis by Photon Observation," *Nucl. Sci. Eng.*, **24**, pp. 184-192.

Gelinas, R.J., S.K. Doss, J.P. Ziagos, P. McKereghan, T. Vogele, and R.G. Nelson (1995), *A New Breed of Innovative Ground Water Modeling*, Lawrence Livermore National Laboratory, Livermore, Calif. (UCRL-JC-120613).

Gelinas, R.J., and R.K. Osborn (1967), "Kinetic Theory for the Interpretation of Measurements on Fluctuations in Radiation Distributions in Finite, Inhomogeneous Systems," *Phys. Rev.*, **163**, No. 1, pp. 162-174.

Hadamard, J. (1952), *Lectures on Cauchy's Problem in Linear Partial Differential Equations*, Dover, Mineola, NY.

Hantush, M.S., and C.E. Jacob (1955), "Non-Steady Radial Flow in an Infinite Leaky Aquifer," *Am. Geophys. Union Trans.*, **26**(1), pp. 95-100.

Hantush, M.S. (1960), "Modification of the Theory of Leaky Aquifers," *The J. of Geophys. Res.*, **65**, pp. 3173-3725.

Jea, K.C., and D.M. Young (1983), "On the Simplification of Generalized Conjugate Gradient Methods for Nonsymmetrizable Linear Systems," Linear Algebra and It's Applications, 52/53, pp. 399-417.

John, F. (1982), *Partial Differential Equations*, Springer-Verlag, New York, NY.

Kitanidis, P.K., and E.G. Vomvoris (1983), "A Geostatistical Approach to the Inverse Problem in Groundwater Modeling (Steady State) and One-Dimensional Simulations," *Water Resour. Res.*, **19**(13), pp. 677-690.

Lax, M., (1966), Discussion of Langevin's technique (title unknown), *Rev. Mod. Phys.*, **38**, p. 541.

McGillem, C.D., and G.R. Cooper (1984), *Continuous and Discrete Signal and System Analysis*, Second Ed., Holt, Rinehart, and Winston, New York, NY.

McLaughlin, D., and L.R. Townley (1996), "A Reassessment of the Groundwater Inverse Problem," *Water Resour. Res.*, **32**(5), pp. 1131-1161.

Menke, W. (1989) *Geophysical Data Analysis: Discrete Inverse Theory*, Revised Ed., Academic Press San Diego, CA.

Nelson, R.W. (1961), "In Place Measurement of Permeability in Heterogeneous Media, 2, Experimental and Computational Considerations," *J. Geophys. Res.*, **66**(8), pp. 2469-2478.

Nelson, R.W. (1962), "Conditions for Determining Areal Permeability Distributions by Calculation," *J. Soc. Petrol. Eng.*, **2**(3), pp. 223-224.

Nelson, R.G. (1998), See Web Page: www.pdesolutions.com., Sunol, CA.

Neuman, S.P. (1973), "Calibration of Distributed Parameter Groundwater Flow Models Viewed as a Multiple-Objective Decision Process Under Uncertainty," *Water Resour. Res.*, **9,** pp. 1006-1021.

Neuman, S.P., and S. Yakowitz (1979), "A Statistical Approach to the Inverse Problem of Aquifer Hydrology, 1, Theory," *Water Resour. Res.*, **15**(4), pp. 845-860.

Neuman, S.P. (1980), "A Statistical Approach to the Inverse Problem of Aquifer Hydrology, 3. Improved Solution Method and Added Perspective," *Water Resour. Res.*, **16**, pp. 331-346.

Ono, S. (1954), "The Quantum-Statistical Theory of Transport Phenomena-III," *Theoret. Phys.*, (Kyoto), **12**, p. 113.

Ono, S. (1959), "The Boltzmann Equation in Quantum-Statistical Mechanics," in *Proceedings of the International Symposium on Transport Processes in Statistical Mechanics*, p. 229, Interscience Publishers, Inc. New York, NY.

Osborn, R.K. (1963), "Kinetic Equations for Fully Ionized, Inhomogeneous Plasmas," *Phys. Rev.* **130**(6), pp. 2142-2155.

Osborn, R.K., and A.Z. Akcasu (1967), "Intensity Fluctuations of the Radiation from a Dispersive Blackbody," *J. Appl. Physics*, **38**(13), pp. 5165-5172.

Osborn, R.K. (1968), "Stochastic Approach to the Theory of Fluctuations in Plasmas," *The Physics of Fluids*, **11**(3), pp. 595-600.

Osborn, R.K., and M. Natelson (1965), Title of Article Unknown, *J. Nucl. Energy*, Part A/B, **19**, p. 916.

Parker, R.L. (1994), *Geophysical Inverse Theory*, Princeton U. Press, Princeton, NJ.

Protter, M.H., and H.F. Weinberger (1984), *Maximum Principles in Differential Equations*, Springer-Verlag, New York, NY.

Stallman, R.W. (1958), "Numerical Analysis of Regional Water Levels to Define Aquifer Hydrology," *Eos Trans. AGU.*, **37**(4), pp. 451-460.

Sun, N.-Z. (1994), *Inverse Problems in Groundwater Modeling,* Kluwer Acad., Norwell, MA.

Theis, C.V. (1935), "The Relation Between the Lowering of the Piezometric Surface and the Rate and Duration of Discharge of a Well Using Ground-Water Storage," *Am Geophys. Union Trans.*, **16**, pp. 519-524.

Vandenberg, P.M. (1988),"Iterative schemes based on minimization of a uniform error criterion," IEEE Transactions on Antennas and Propagation, AP-36, pp. 1418-1423.

Yeh, W. W-G. (1986), "Review of Parameter Identification Procedures in Groundwater Hydrology: The Inverse Problem," *Water Resour. Res.*, **22**, pp. 95-108.

Zhu, J. (1992), "Using a Hypercube to Solve Inverse Problems in Reservoir Simulations," Applications on Advanced Architecture Computers Section, Greg Astfalk, Editor, *SIAM News*, March, pp. 1-11.

APPENDIX A

Table 1. Transmissivity Data from HSU2

#	X position (ft)	Y position (ft)	Conductivity (gal/ft^2- day)	Transmissivity (gal/ft-day)	Well Name
1	7479.17	10143.18	200.00	12600.00	W-022A
2	6745.90	8731.70	53.00	3869.00	W-102
3	5073.90	9644.20	270.00	15120.00	W-109
4	6848.52	9362.30	240.00	15360.00	W-118
5	10666.28	11386.06	100.00	5500.00	W-119
7	4583.80	10344.70	16.00	880.00	W-149
8	6379.33	9730.17	86.00	5074.00	W-201
10	9444.46	8684.27	110.00	6292.00	W-223
11	10684.81	10723.38	400.00	19880.00	W-224
12	6383.65	9052.80	22.00	1364.00	W-260
14	9133.52	10368.12	100.00	5800.00	W-301
15	9113.88	11003.47	70.00	4060.00	W-303
16	10039.60	10109.00	72.00	4392.00	W-305
17	8291.22	11254.94	68.00	3808.00	W-306
18	7931.70	10457.20	5.40	334.80	W-308
19	10599.00	12696.70	280.00	16940.00	W-316
20	6321.13	8306.25	15.00	930.00	W-322
21	6437.23	11691.87	59.00	3304.00	W-323
22	9913.37	10431.15	17.00	1059.10	W-353
23	7455.20	10645.40	110.00	6820.00	W-357
24	10129.60	11808.80	96.00	6240.00	W-369
25	4411.70	10110.20	530.00	29680.00	W-404
27	9948.48	12179.87	83.00	4731.00	W-411
28	6461.63	11160.69	42.00	2688.00	W-422
29	10186.56	12772.32	130.00	7930.00	W-423
30	7056.85	8746.98	600.00	45600.00	W-448
31	7390.99	8237.85	16.00	1120.00	W-451
32	5691.93	9385.83	24.00	1416.00	W-457
33	8452.06	8843.66	53.00	4028.00	W-464
34	9172.52	13185.18	30.00	1830.00	W-486
35	8916.54	9336.88	88.00	4928.00	W-551
36	5072.25	9525.37	150.00	8400.00	W-544

Table 2. Head Data from HSU2

#	X position (ft)	Y position (ft)	Head (h) (ft)	Well Name
1	7526.00	9120.70	532.30	W-001
3	7479.20	10143.20	536.20	W-002A
4	7588.20	13841.20	537.90	W-005A
5	10820.90	13421.60	551.90	W-007
6	10186.00	11268.00	546.50	W-010A
7	10164.70	9285.40	541.00	W-012
8	6745.90	8731.70	530.10	W-102
9	5073.90	9644.20	527.40	W-109
10	8466.90	8745.50	534.60	W-111
11	6848.50	9362.30	530.80	W-118
12	10666.30	11386.10	549.60	W-119
13	4538.90	9680.20	526.40	W-120
14	4200.60	9114.70	525.50	W-121
15	11400.30	11438.00	551.20	W-142
17	8353.00	9406.00	535.50	W-146
18	4583.80	10344.70	526.30	W-149
19	4593.90	11573.40	525.60	W-150
20	3493.60	10826.80	523.40	W-151
21	6379.30	9730.20	530.20	W-201
22	8961.10	7661.90	535.70	W-202
23	11401.50	10143.50	574.80	W-204
24	11335.60	10897.60	550.60	W-207
27	11287.50	11815.20	551.40	W-222
28	9444.50	8684.30	537.70	W-223
29	10684.80	10723.40	546.90	W-224
30	7967.40	8783.30	533.40	W-252
31	8661.20	8017.30	534.50	W-253
32	10922.40	10170.90	545.80	W-257
33	10954.30	9755.40	545.50	W-259
34	6383.60	9052.80	529.80	W-260
35	7208.60	8927.60	531.60	W-263
37	10572.70	10126.90	544.20	W-271
38	10517.20	9687.30	543.10	W-272
39	11213.60	12165.90	551.70	W-273
40	11154.30	9382.50	546.30	W-274
41	9133.50	10368.10	539.30	W-301
42	9113.90	11003.50	540.30	W-303
43	10039.60	10109.00	542.00	W-305
44	8291.20	11254.90	538.20	W-306
45	7931.70	10457.20	535.50	W-308
46	10629.40	12349.10	549.70	W-313
47	10599.00	12696.70	549.70	W-316

Table 2. Head Data from HSU2 (Continued)

#	X position (ft)	Y position (ft)	Head (h) (ft)	Well Name
48	9331.90	11817.40	543.20	W-317
49	11183.40	12586.60	553.50	W-318
50	9149.40	12573.20	543.40	W-320
51	6321.10	8306.20	529.60	W-322
52	6437.20	11691.90	532.10	W-323
53	9913.40	10431.20	542.90	W-353
54	10665.70	12056.80	549.60	W-355
55	7455.20	10645.40	534.20	W-357
56	7057.90	11051.40	533.50	W-365
57	10129.60	11808.80	547.10	W-369
58	9624.80	12960.40	545.50	W-375
59	7570.70	8701.80	532.30	W-376
60	4734.70	9695.60	526.80	W-377
61	4904.10	9641.50	527.20	W-378
62	4907.00	9491.30	527.50	W-379
63	2925.40	10356.90	523.80	W-401
64	4411.70	10110.20	525.80	W-404
65	3241.90	9650.00	524.60	W-405
66	9948.50	12179.90	546.40	W-411
67	8619.10	11966.90	540.70	W-413
70	7482.80	10474.10	534.10	W-420
71	6461.60	11160.70	531.20	W-422
72	10186.60	12772.30	548.20	W-423
73	7056.90	8747.00	530.20	W-448
75	7391.00	8237.80	531.70	W-451
76	7512.50	12423.10	537.50	W-453
78	5691.90	9385.80	528.50	W-457
79	7423.50	10991.20	534.40	W-458
80	5689.90	8762.70	528.30	W-460
81	8452.10	8843.70	534.70	W-464
82	7356.90	8734.60	530.80	W-482
84	7159.00	8513.10	530.90	W-485
85	9172.50	13185.20	544.10	W-486
87	6833.40	11909.50	533.60	W-507
88	8916.50	9336.90	537.00	W-551
89	5072.50	9525.40	527.30	W-554
90	7655.50	6992.90	532.00	W-557
91	7926.30	7075.80	532.50	W-591
92	8177.10	7233.40	533.10	W-592
93	11359.30	13373.70	556.50	W-594

Technical Information Department • **Lawrence Livermore National Laboratory**
University of California • Livermore, California 94551